International Journal of Coal Geology 287 (2024) 104508

Contents lists available at ScienceDirect

International Journal of Coal Geology

journal homepage: www.elsevier.com/locate/coal

Geochemical characteristics and formation mechanism of organic-rich source rocks of mixed sedimentary strata in continental saline lacustrine basin: A case study of Permian Pingdiquan formation in the Shishugou Sag, Junggar Basin, Northwest China

Wenren Zeng [a,b,c,d], Boran Wang [a,b], Xuan Chen [e], Guobin Fu [e], Zhihuan Zhang [a,b,*], Zhilong Huang [a,b]

[a] State Key Laboratory of Petroleum Resources and Prospecting, China University of Petroleum (Beijing), Beijing 102249, China
[b] College of Geoscience, China University of Petroleum, Beijing 102249, China
[c] Oil & Gas Survey, China Geological Survey, Beijing 100083, China
[d] The Key Laboratory of Unconventional Petroleum Geology, China Geological Survey, Beijing 100083, China
[e] PetroChina Tuha Oilfield Company, Hami 839009, China

A R T I C L E I N F O

Keywords:
Saline lacustrine basin
Inorganic geochemistry
Molecular geochemistry
Depositional environment
Paleoproductivity
Formation mechanism

A B S T R A C T

The Permian Pingdiquan Formation (P_2p) in Shishugou Sag, Junggar Basin, Northwest China, is a typical example of mixed sedimentary strata formed in a saline lacustrine environment, characterized by complex lithological assemblages and extensive distribution of organic-rich source rocks. To further investigate the differences in oil-source contribution and hydrocarbon generation characteristics of source rocks with different lithologies, studying the difference of their geochemical characteristics and the formation mechanism of organic-rich source rocks is the top priority. Based on a comprehensive analysis of lithologic types, geochemical characteristics, and hydrocarbon generation potential of source rocks using organic petrology, molecular geochemistry and element geochemistry, this paper reveals the formation background and organic matter enrichment mechanism of the P_2p organic-rich source rocks. The results show that the mixed sedimentary rocks of the P_2p were deposited under relatively arid and saline lacustrine conditions. Paleoclimatic conditions tended to be more arid and hydrothermal activity became more frequent during the sedimentation process from mudstone, dolomitic mudstone to argillaceous dolomite. Consequently, the water column salinity elevated, leading to an increased proportion of salt-tolerant green algae and slight salt-tolerant cyanobacteria compared to salt-intolerant algae. Frequent changes in paleoclimate and hydrothermal activity control the interbedding deposition of mudstone, dolomitic mudstone and argillaceous dolomite, and the resulting salinity fluctuations contribute to variations in the proportion of salt-tolerant and intolerant algae in source rocks with different lithologies. Furthermore, the source rocks within the mixed sedimentary strata (mudstone, dolomitic mudstone and argillaceous dolomite) all exhibit substantial hydrocarbon generation potential, and there exists heterogeneity among source rocks of the same lithology. The key factor influencing the development of these organic-rich source rocks is the enhancement of palaeoproductivity driven by volcanic activity. Additionally, the water stratification caused by saline water promotes anoxic water columns, also contributing to organic matter enrichment in the source rocks.

1. Introduction

Mixed sedimentation refers to a distinctive sedimentary phenomenon where different types of sediments (such as terrigenous clastic and carbonate materials) are intermingled within the same depositional environment, which can occur in both marine and continental settings (Mount, 1984; Davis et al., 2003; Xia et al., 2019). Coastal and shallow marine sedimentary environments favor the development of mixed

* Corresponding author at: State Key Laboratory of Petroleum Resources and Prospecting, China University of Petroleum (Beijing), Beijing 102249, China.
E-mail address: zhangzh3996@vip.163.com (Z. Zhang).

https://doi.org/10.1016/j.coal.2024.104508
Received 19 October 2023; Received in revised form 26 March 2024; Accepted 8 April 2024
Available online 16 April 2024
0166-5162/

sediments, while in continental sedimentary environments, it is challenging to develop mixed sediments except in saline lake environments (Mount, 1984; Dorsey and Kidwell, 1999; Feng et al., 2013). In recent years, with the increasing focus on unconventional oil and gas exploration, it has been demonstrated that mixed sedimentary strata play a significant role in the enrichment of unconventional hydrocarbon resources (Zou et al., 2013; Katz and Lin, 2014; Wu et al., 2016; Hu et al., 2018b; Zhang et al., 2019b). Consequently, the study of mixed sedimentary strata holds immense significance for the exploration and development of unconventional oil and gas resources. However, the majority of current research primarily focuses on mixed sediments in marine environments, while studies on source rocks within mixed sedimentary strata in continental saline lake environments remain relatively limited (Vandeginste et al., 2009; Warren, 2010; Xiao et al., 2020; Jiang et al., 2021; Song et al., 2021; Xiao et al., 2021; Rodrigues et al., 2022).

Previous studies have demonstrated the presence of abundant unconventional oil and gas resources associated with mixed sedimentation in numerous saline lake basins across China, including the Permian Lucaogou Formation in Jimusar Sag and Santanghu Basin (Wu et al., 2016; Pan et al., 2021), the Paleogene Funing Formation in Subei Basin (Liu et al., 2020), the Paleogene Xingouzui Formation in Jianghan Basin (Li et al., 2015), and the Paleogene Hetaoyuan Formation in Nanxiang Basin (Xia et al., 2019). The mixed sedimentary rocks formed in these saline lake basins exhibit significant hydrocarbon generation potential, serving as the fundamental oil source material for the formation of large-scale oil and gas fields as well as unconventional oil and gas resources (Liu et al., 2017; Hou et al., 2017; Song et al., 2019; Song et al., 2021; Chang et al., 2023). The formation of organic-rich source rocks in mixed sedimentary strata is typically closely linked to paleoproductivity, organic matter preservation conditions, and paleoclimate conditions (Pan et al., 2020; Tang et al., 2020; Song et al., 2021; Meng et al., 2022), and generally exhibits the following common characteristics. Firstly, the relatively arid paleoclimate conditions play an essential role in the development of saline lake basins, facilitating the formation of mixed sedimentary strata. Secondly, the paleoproductivity and organic matter preservation conditions generally influence the organic matter enrichment in source rocks (Eugster and Hardie, 1978; Katz, 2005; Hu et al., 2018a; Xie et al., 2021; Zeng et al., 2023b). However, the geochemical characteristics and formation mechanisms of organic-rich source rocks in mixed sedimentary strata across different basins may exhibit significant variations (Hu et al., 2018a; Xia et al., 2019; Pan et al., 2020; Li et al., 2021; Tao et al., 2022).

Compared to the Jianghan Basin and Nanxiang Basin, the mixed sedimentary rocks of the Permian Pingdiquan Formation (P_2p) in the Shishugou Sag exhibit distinct uniqueness and complexity. The source rock is mainly characterized by mudstone, dolomitic mudstone and argillaceous dolomite formed against a background of volcano-hydrothermal activities (Li et al., 2021; Fan et al., 2021). The source rocks of the mixed sedimentary strata of the P_2p in Shishugou Sag have high hydrocarbon generation potential with the highest TOC reaching up to 11.12%, and the source of organic matter is mainly aquatic organisms such as algae (Zeng et al., 2023a). Therefore, it is a set of organic-rich mixed sedimentary rocks formed in saline lake basins and influenced by volcano-hydrothermal activities (Li et al., 2021; Fan et al., 2021; Zeng et al., 2023a). Currently, the lithological characteristics and formation mechanisms of organic-rich source rocks in the mixed sedimentary strata of continental saline lake basins remain unclear, and there are still unresolved issues in related research (Palermo et al., 2008; Liu et al., 2017; Li et al., 2021). For instance, the impact of salinity on algal growth or algal population diversity in lake basins controlled by paleoclimate conditions remains unclear. Furthermore, most studies treat mudstone, dolomitic mudstone and argillaceous dolomite as a whole, without adequately acknowledging the variations in formation mechanisms among source rocks with different lithologies (Palermo et al., 2008; Feng et al., 2013; Liu et al., 2017; Li et al., 2021; Jiang et al., 2021). This has limited the exploration progress of unconventional oil and gas associated with mixed sedimentation. Therefore, further investigation into the formation mechanism of organic-rich mixed sedimentary rocks of the P_2p is imperative.

This study employed a comprehensive approach combining mineralogy, organic petrology, molecular geochemistry and inorganic geochemistry to systematically investigate the sedimentary environment and source of organic matter of the P_2p mixed sedimentary rocks in the Shishugou Sag. The primary objective of this study is to elucidate the differences in the formation environment of the source rocks with varying lithologies within the mixed sedimentary strata in the study area, and to reveal the formation mechanisms and main controlling factors of the organic-rich source rocks. The research findings will serve as a crucial foundation for subsequent oil and gas exploration and development in the Shishugou Sag, while also enhancing comprehension of the formation mechanism of organic-rich source rocks in mixed sedimentary strata found in saline lake basins.

2. Geological setting

The Junggar Basin, located in northwest China, is a superimposed basin with abundant oil and gas resources (Fig. 1a) (Xiang et al., 2015; Tao et al., 2016; Yu et al., 2017). The eastern uplift belt of the Junggar Basin is located between Kelameili mountain and Bogda mountain, with an approximate area of 3×10^4 km^2. The Kelameili mountain subducted northward during the Late Early Devonian and subsequently closed in the Early Carboniferous, resulting in the formation of a foreland basin. During the Middle Permian, the eastern region of the Junggar Basin experienced post-orogenic stress relaxation, forming multiple depositional centers located between the Kelamili and Bogda mountains. Additionally, the Shaqi uplift in the middle section acted as a barrier, separating various north-south depressions. During the Indonesian, Yanshan and Himalayan orogenies, the NE-SE compressive stress exerted significant influence on fault activity, resulting in the development of major fault systems controlling structural belts and local structures, ultimately leading to the formation of the current “checkerboard” tectonic pattern characterized by alternating depressions and uplifts (Luo et al., 2007; Xiao et al., 2008). The Shishugou Sag is located in the northwestern region of the “checkerboard” tectonic pattern, adjacent to the Shazhang fault-fold belt towards the west, Huangcaohu uplift towards the east, Kelameili mountain towards the north, and Shaqi uplift towards the south (Fig. 1b, c).

The sedimentary strata in the Shishugou Sag are arranged in a sequence from bottom to top, including Carboniferous, Permian, Triassic, Jurassic, and Cretaceous (Fig. 1d). The Permian system in the Shishugou Sag comprises the Middle Permian Jiangjunmiao Formation (P_2j), the Middle Permian Pingdiquan Formation (P_2p), and the Upper Permian Wutonggou Formation(P_3wt). From bottom to top, the P_2p is subdivided into three members (P_2p^1, P_2p^2, and P_2p^3). According to previous studies, P_2p^1 and P_2p^2 of the Shishugou Sag exhibit high organic matter abundance (TOC > 2.0%) of source rocks. Moreover, the stratas have relatively better reservoir properties and oiliness due to its high dolomite content (Zhang et al., 2021). Therefore, based on the organic matter abundance of source rocks, reservoir characteristics, and oiliness, the P_2p^1 and P_2p^2 are considered the “sweet spot” of the P_2p in Shishugou Sag and are the target layer of this study. The “sweet spot” of the P_2p exhibits a consistent thickness distribution ranging from 50 to 100 m (Fig. 1d) (Zhang et al., 2021). The unit was deposited in saline shallow and semi-deep lake environments, serving as the development layer for organic-rich source rocks within the P_2p. The lithology of the source rock is characterized by a complex mixture of terrigenous clastic and carbonate materials. In addition, the P_2p^3 exhibits large stratigraphic thickness and was deposited in a regional shallow lacustrine environment, while displaying a significantly low organic matter abundance in the source rock.

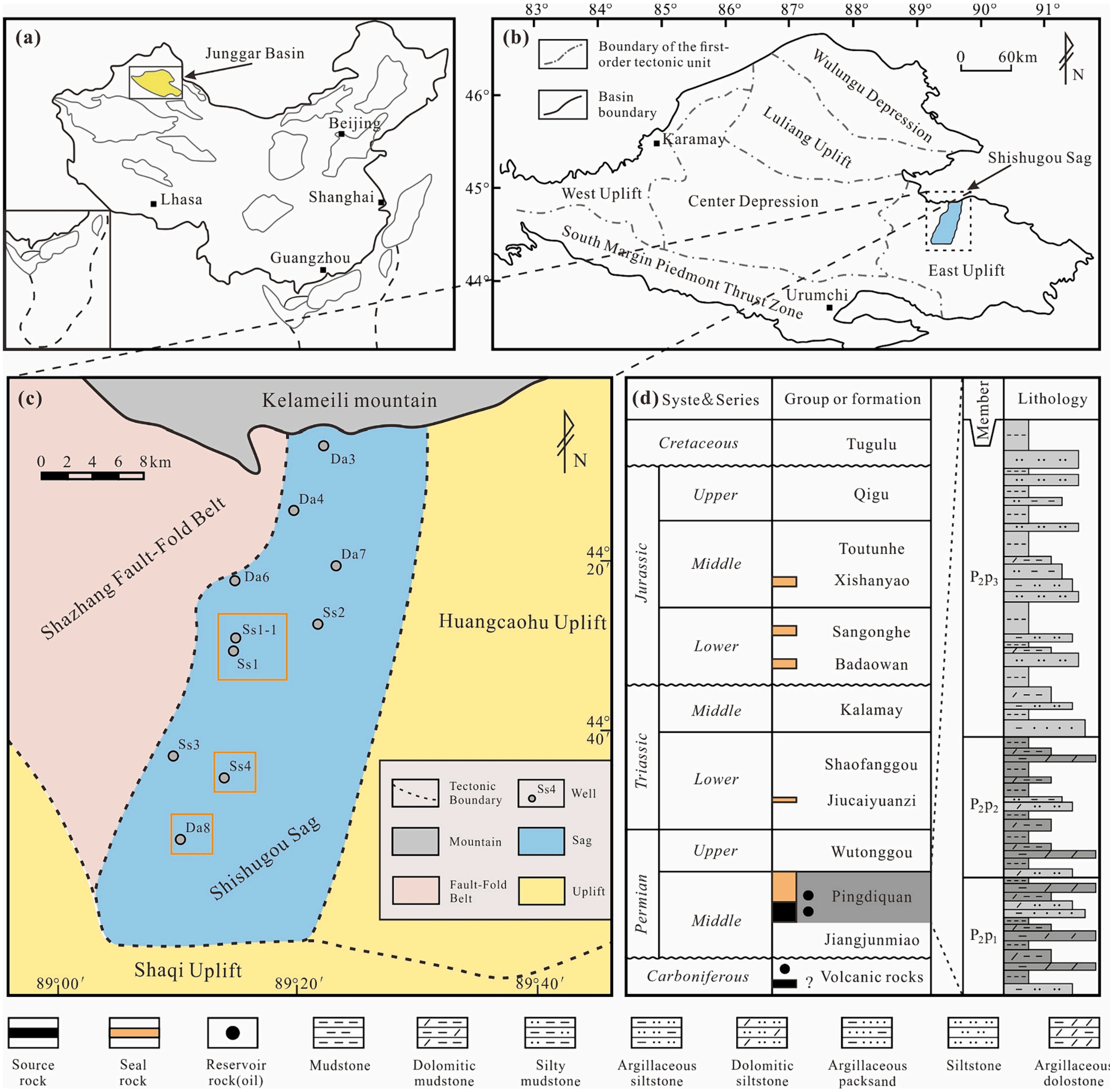

Fig. 1. Structure location map and stratigraphic column of the Shishugou Sag, Junggar Basin (Zhang et al., 2021). (a) Location of the Junggar Basin in China; (b) Location of the Shishugou Sag in Junggar Basin; (c) Tectonic units of the Shishugou Sag with the location of the sampling well (orange rectangle); (d) Stratigraphy of the Pingdiquan Formation in the Shishugou Sag.

3. Samples and methods

In this study, all core samples were selected from Members 1 and 2 of the Middle Permian Pingdiquan Formation (P_2p) obtained from four wells in Shishugou Sag (Fig. 1c), including 24 mudstones, 19 dolomitic mudstones and 12 argillous dolomites. All samples underwent Rock-Eval pyrolysis, total organic carbon (TOC) and XRD (X-ray diffraction) analysis. Furthermore, a subset of samples were selected for organic petrographic analysis, gas chromatography–mass spectrometry (GC–MS) of saturated hydrocarbon and elemental analysis. The element geochemistry analysis was conducted at the Analytical Laboratory of the Beijing Research Institute of Uranium Geology, China. Other experiments were carried out at the State Key Laboratory of Petroleum Resources and Prospecting at the China University of Petroleum (Beijing).

3.1. X-ray diffraction

Before to conducting the XRD measurements, samples were pulverized to a particle size of −200 mesh and subjected to analysis using a Bruker D8 Focus X-ray diffractometer in accordance with the Chinese oil and natural gas industry standard SY/T 5163–2018. The experimental conditions were maintained at 24 °C and relative humidity at 35%. During the experiment, each scan was performed from 5° to 65°2θ, with a step size of 0.02° and a rate of 2.0°/min. The X-ray source is Cu-Kα radiation. The quantitative analysis of the mineral composition of each powder sample is carried out by using MDI Jade X-ray Diffraction software.

3.2. Bulk geochemistry

The TOC was tested by a LECO CS-230 instrument. The sample was subjected to pretreatment using a dilute hydrochloric acid solution (5%)

in order to eliminate the presence of inorganic carbon. Rock-Eval pyrolysis was analyzed using a Rock-Eval 6 pyrolysis instrument, which heated at 300 °C for 3 min and gradually increased to 650 °C for 14 min. These two experiments followed the Chinese National Standard GB/T19145–2022 and GB/T18602–2016, respectively.

3.3. Maceral and vitrinite reflectance analysis

The organic petrography analysis was conducted using a Leica DM 4500P microscope, enabling oil immersion ×50 objective observation and statistical analysis under both reflected 'white' light and UV (ultraviolet) light to determine the maceral composition. To ensure experimental accuracy, each sample measurement included at least 500 points. Vitrinite reflectance (Ro) was determined using a microphotometer (MV-SP), with at least 50 measurements taken for each sample.

3.4. Molecular biomarkers analysis

The saturated hydrocarbon fractions were analyzed using an Agilent 6890 Gas Chromatograph (GC) equipped with the HP-5MS column and linked with an Agilent 5975i Mass Spectrometer (MS), according to Chinese National Standard GB/T 18606–2017. The temperature gradient heating method ranged from 50 to 310 °C, with a heating rate of 4 °C/min. Each sample underwent testing for approximately 70 min.

3.5. Major oxides and trace elemental (ICP-MS) analyses

Major oxides were analyzed using an Axios-mAX X-ray fluorescence (XRF) spectrometer according to Chinese National Standard GB/T 14506.28–2010. The trace elements were analyzed using inductively coupled plasma mass spectrometry (ICP-MS) following the Chinese National Standard GB/T 14506.30–2010. The dried samples were dissolved in a mixture of 30% HF and 68% HNO_3 in capped Teflon bombs at 150 °C for 48 h. Subsequently, the residual material was treated with 2 ml of concentrated nitric acid, followed by dissolution in a 50 ml solution using 5% diluted nitric acid. The precision and accuracy of the ICP-MS and X-ray fluorescence data are reported by Cullen et al. (2001), Qian et al. (2009), Wu et al. (2010) and Roser et al. (1995).

4. Results

4.1. Mineralogical characteristics

The XRD analysis reveals that the mixed sedimentary rocks of the P_2p in Shishugou Sag predominantly consist of quartz (5–45%, avg. 25.42%), plagioclase (9–54%, avg. 27.65%), dolomite (2–75%, avg. 30.31%) and clay minerals (1–33%, avg. 9.56%), with relatively low content of potassium feldspar (0–14%, avg. 2.44%), calcite (0–5%, avg. 0.29%), siderite (0–8%, avg. 1.93%), pyrite (0–5%, avg. 0.82%) and analcite (0–14%, avg. 1.58%) (Table 1). The constituent of carbonate minerals is mainly dolomite, with a minor presence of calcite. Additionally, the mineral composition of source rocks shows significant variations across different lithologies. The dolomite content (avg. 11.71%, avg. 34.11%, avg. 61.50%) progressively increases in mudstone, dolomitic mudstone and argillaceous dolomite. Whereas the average content of clay minerals (avg. 12.21%, avg. 9.42%, avg. 4.50%), quartz (avg. 33.88%, avg. 21.84%, avg. 14.17%) and plagioclase (avg. 34.08%, avg. 27.63%, avg. 14.83%) decreases successively for these lithologies (Table 1).

4.2. Total organic carbon content and programmed temperature pyrolysis data

The sedimentary strata of the P_2p in the study area consist primarily of mudstone, dolomitic mudstone and argillaceous dolomite, with abundant organic-rich source rocks present within these lithologies. Most samples have TOC and $S_1 + S_2$ values exceeding 1.0% and 5.0 mg/g, respectively (Table 2), and the source rock quality, based on organic matter abundance, within these mixed sedimentary rocks ranges from good to excellent (Fig. 2a). The TOC values of mudstone, dolomitic mudstone and argillaceous dolomite are 0.79–12.04% (avg. 5.33%), 0.51–9.67% (avg. 4.92%), 1.24–9.66% (avg. 5.23%), respectively (Table 2), and the $S_1 + S_2$ values are 3.33–92.12 mg/g (avg. 34.34 mg/g), 1.97–66.59 mg/g (avg. 30.12 mg/g), 6.65–77.35 mg/g (avg.34.72 mg/g), respectively (Table 2).

The hydrogen index (HI), which indicates the hydrocarbon generation potential, shows no significant differences among the different lithologies (Fig. 2b). The HI values of mudstone, dolomitic mudstone and argillaceous dolomite are 335–809 mg HC/g TOC (avg. 552 mg HC/g TOC), 311–825 mg HC/g TOC (avg. 541 mg HC/g TOC) and 341–787 mg HC/g TOC (avg. 559 mg HC/g TOC), respectively (Table 2). According to the results of pyrolysis data analysis, the kerogen of most source rocks is type I-II_1 (Fig. 2b).

The source rocks of the P_2p fall into the low mature to mature stage (Fig. 2b). It is worth noting, however, that T_{max} for lacustrine OM, particularly very hydrogen rich OM derived from algae, often has a higher T_{max} value at very low maturities than similarly oil prone and immature marine source rocks. For example, the T_{max} values for fully immature oil shales of the Green River Formation regularly approach 440 °C (Horsfield et al., 1994). Therefore, through a comprehensive analysis of vitrinite reflectance in "*4.3. Maceral composition*" and biomarker parameters in "*4.4. Biomarker compound characteristics*", we concluded that the P_2p source rocks predominantly in the low maturity stage.

In summary, the mudstone, dolomitic mudstone and argillaceous dolomite of the P_2p have high organic matter abundance and mainly

Table 1
Mineral composition of source rock samples from the P_2p, Shishugou Sag, Junggar Basin.

Lithology	Statistical value	Clay (%)	Quartz (%)	Potash feldspar (%)	Plagioclase (%)	Calcite (%)	Dolomite (%)	Siderite (%)	Pyrite (%)	Analcite (%)
Mudstone (*N* = 24)	Minimum	4	22	0	17	0	2	0	0	0
	Maximum	25	45	14	54	3	22	8	5	14
	Mean	12.21	33.88	2.58	34.08	0.13	11.71	2.13	1.00	2.29
Dolomitic mudstone (*N* = 19)	Minimum	3	10	0	10	0	26	0	0	0
	Maximum	33	39	12	40	5	45	6	3	9
	Mean	9.42	21.84	3.05	27.63	0.32	34.11	1.63	0.63	1.37
Argillaceous dolomite (*N* = 12)	Minimum	1	5	0	9	0	53	0	0	0
	Maximum	16	25	5	23	3	75	8	4	2
	Mean	4.50	14.17	1.17	14.83	0.58	61.50	2.00	0.75	0.50
All samples (*N* = 55)	Minimum	1	5	0	9	0	2	0	0	0
	Maximum	33	45	14	54	5	75	8	5	14
	Mean	9.56	25.42	2.44	27.65	0.29	30.31	1.93	0.82	1.58

"N" is the number of source rock samples.

Table 2
Total organic carbon, Rock-Eval pyrolysis and organic maceral data of source rock samples from the P_2p, Shishugou Sag, Junggar Basin.

Lithology	Statistical value	TOC	S_1	S_2	$S_1 + S_2$	HI	T_{max}	Ro	Endogenous OM	Terrigenous OM
Mudstone (N = 24)	Minimum	0.79	0.21	3.12	3.33	334.63	428	0.66	47.62	5.41
	Maximum	12.04	6.59	85.90	92.12	808.81	450	0.78	94.59	52.38
	Mean	5.33	2.83	31.51	34.34	551.69	442	0.72	74.99	25.01
Dolomitic mudstone (N = 19)	Minimum	0.51	0.17	1.70	1.97	310.98	430	0.66	61.28	13.22
	Maximum	9.67	5.22	61.48	66.59	824.68	448	0.78	86.78	38.72
	Mean	4.92	1.98	28.14	30.12	540.62	441	0.72	74.17	25.83
Argillaceous dolomite (N = 12)	Minimum	1.24	1.23	5.42	6.65	340.51	433	0.65	51.56	10.86
	Maximum	9.66	5.22	76.03	77.35	787.06	452	0.76	89.14	48.44
	Mean	5.23	2.71	32.01	34.72	558.92	440	0.71	70.41	29.60
All samples (N = 55)	Minimum	0.51	0.17	1.70	1.97	310.98	428	0.65	47.62	5.41
	Maximum	12.04	6.59	85.90	92.12	824.68	452	0.78	94.59	52.38
	Mean	5.17	2.51	30.45	32.96	549.44	441	0.72	73.60	26.40

"N" is the number of source rock samples. 1. TOC: total organic carbon (wt%); 2. S_1: free hydrocarbons (mg HC/g rock); 3. S_2: hydrocarbons generated during Rock Eval pyrolysis (mg HC/g rock); 4. $S_1 + S_2$: generative potential (mg HC/g rock); 5. HI: hydrogen index = $(S_2/TOC) \times 100$, (mg HC/g TOC); 6. T_{max} = temperature with maximum hydrocarbon generation (°C); 7. Ro: vitrinite reflectance (%); 8. Endogenous OM: endogenous organic maceral includes lamalginite and telalginite, vol%, mmf; 9. Terrigenous OM: terrigenous organic maceral includes sporinite, vitrinite and inertinite, vol%, mmf.

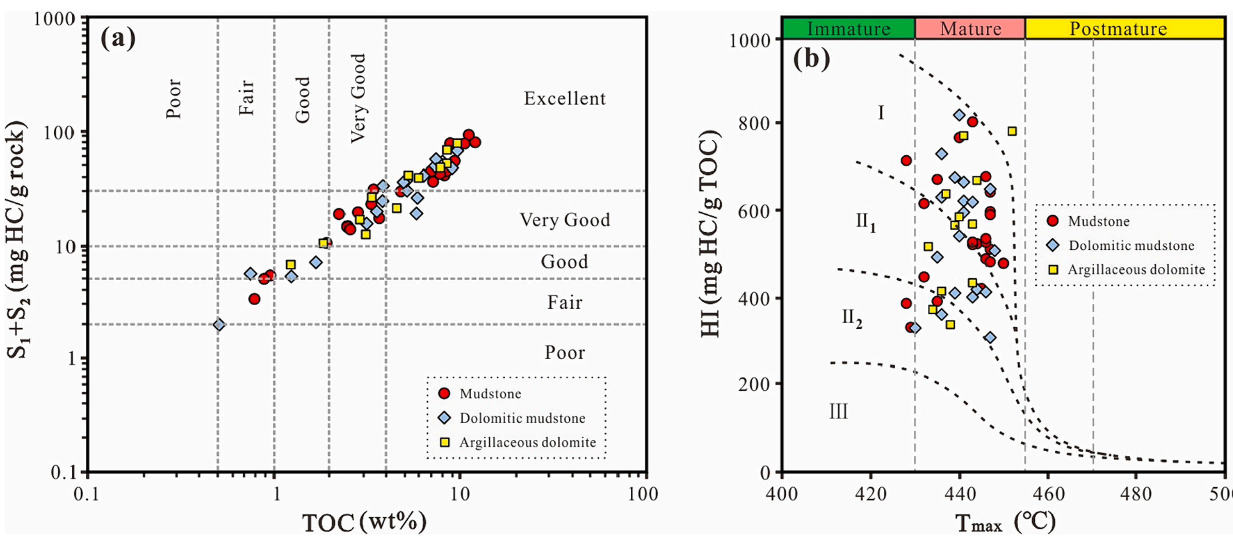

Fig. 2. (a) The crossplots of TOC versus ($S_1 + S_2$) of source rock samples from the P_2p, Shishugou Sag, Junggar Basin (according to Peters and Cassa, 1994); (b) The crossplot of T_{max} versus hydrogen index of source rock samples from the P_2p, Shishugou Sag, Junggar Basin (according to Peters and Cassa, 1994).

contain type I-II_1 kerogen within the thermally low mature zone. The above experimental data (Table 2 and Fig. 2a) also indicates that while there is minimal variation in the average organic matter abundance among source rocks with different lithologies, there exists evident heterogeneity in the organic matter abundance within source rocks of the same lithology.

4.3. Maceral composition

Abundant organic macerals, including varying proportions of vitrinite, liptinite and inertinite, are observed in the microscopic photos of the P_2p mixed sedimentary rocks in the study area (Table 2; Fig. 3). The liptinite of the P_2p source rocks mainly consists of telalginite, lamalginite and sporinite, with a particularly minimal presence of cutinite, resinite, suberinite and exsudatinite. To discuss the origin of organic matter more clearly and accurately, the organic maceral is classified into two distinct categories: endogenous OM and terrigenous OM. Among them, the endogenous OM mainly includes telalginite and lamalginite, indicating the source of aquatic organic matter in the lake basin (Xie et al., 2014; Pickel et al., 2017). The terrigenous OM comprises sporinite, vitrinite and inertinite, representing the sources of terrestrial higher plant organic matter (Xie et al., 2014; Pickel et al., 2017; ICCP, 1998, 2001).

The average content of endogenous OM (47.62–94.59 vol%, avg. 73.60 vol%) in the P_2p source rocks is significantly higher than that of terrigenous OM (5.41–52.38 vol%, avg. 26.40 vol%), and there is no significant variation observed in the composition of endogenous OM among different lithologies. The content of endogenous OM in mudstone, dolomitic mudstone and argillaceous dolomite (47.62–94.59 vol%, avg. 74.99 vol%; 61.28–86.78 vol%, avg. 74.17 vol%; 51.56–89.14 vol%; avg. 70.41 vol%) is higher than that of terrigenous OM (5.41–52.38 vol%; avg. 25.01 vol%; 13.22–38.72 vol%, avg. 25.83 vol%; 10.86–48.44 vol%, avg. 29.60 vol%), respectively (Table 2). The data demonstrates that endogenous OM constitutes the primary component of source rock organic matter. Furthermore, although there is no significant disparity in the average relative content of organic macerals among source rocks with different lithologies, a substantial variation exists in the distribution range of endogenous OM and terrigenous OM within source rocks of the same lithology.

The alginite of the P_2p source rocks predominantly consists of lamalginite with strong yellow-green fluorescence (Fig. 3b), while the telalginite is less abundant and shows strong yellow-green fluorescence (Fig. 3d). The sporinite is observed as slender strips with smooth margins, typically occurring individually with yellow-light yellow fluorescence (Fig. 3b, d). The vitrinite particles are small and irregularly shaped (Fig. 3a, c). It can be observed that vitrinite is within numerous pyrite

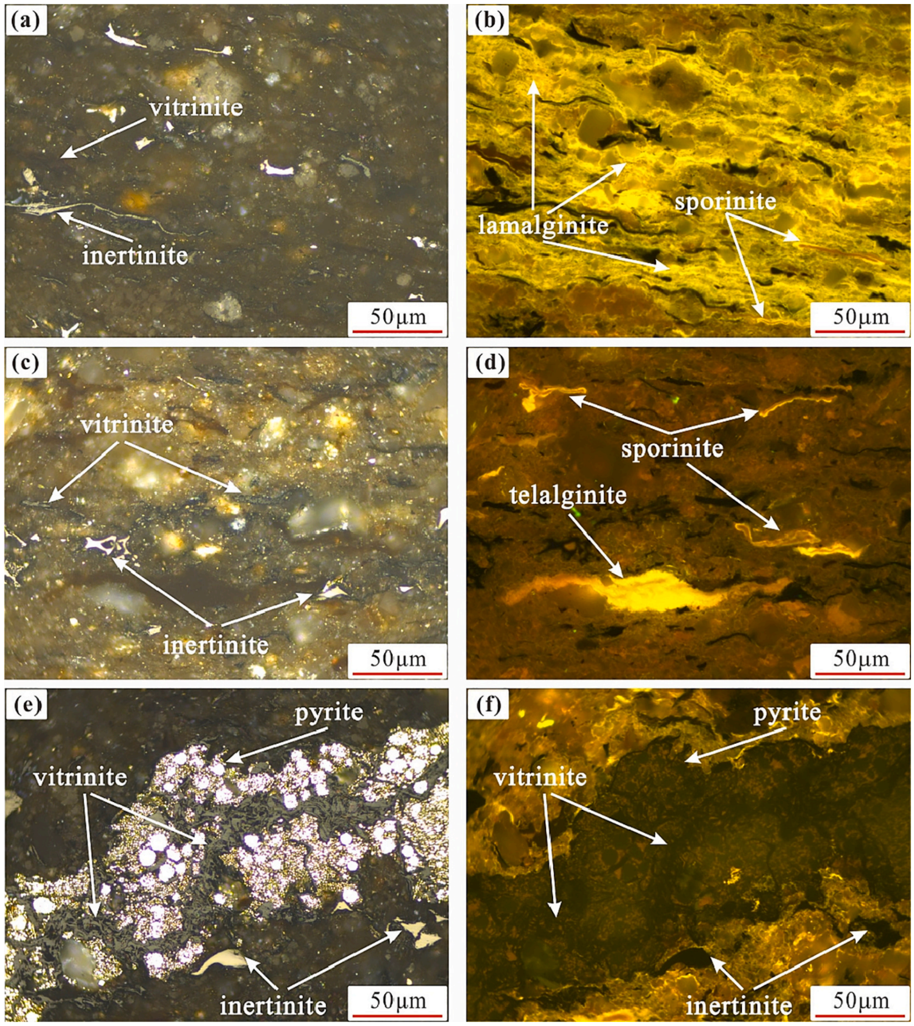

Fig. 3. Representative maceral Photomicrographs of source rock samples from the P_2p, Shishugou Sag, Junggar Basin. (a-b) inertinite, vitrinite, lamalginite and sporinite, under reflected 'white' light and UV light; (c-d) inertinite, telalginite and sporinite, under reflected 'white' light and UV light; (e-f) pyrite, vitrinite and inertinite, under reflected 'white' light and UV light.

particles in some samples (Fig. 3e, f), indicating well-preserved terrigenous organic matter deposited in a reducing water column. Under reflected white light, vitrinite occurs as gray or dark gray (Fig. 3a, c, e, f), while inertinite occurs as bright dispersed particles in the mineral matrix (Fig. 3a, c, e). The vitinite reflectance of the P_2p source rocks ranges from 0.65 to 0.78% (avg. 0.72%), reflecting an early stage of maturity (Table 2).

4.4. Biomarker compound characteristics

4.4.1. Normal alkanes, isoprenoids

The P_2p source rocks primarily contain short-chain n-alkanes, with the highest abundance in the range of n-C_{19} to n-C_{23} (Fig. 4a, b, c). The values of the carbon preference index (CPI) range from 1.09 to 1.48 (avg. 1.25), and the ratios of $\Sigma nC_{21}^{-}/\Sigma nC_{22}^{+}$ range from 0.60 to 1.95 with an average of 1.12 (Table 3). All source rock samples contain abundant pristane (Pr) and phytane (Ph). The ratios of Pr/Ph range from 0.95 to 1.95 (avg. 1.40), exhibiting minimal variation among source rocks with different lithologies (Table 3).

4.4.2. β–carotane

Abundant β-carotane was detected in the majority of source rock samples (Table 3, Fig. 4a, b, c). Furthermore, there is a significant variation in the β-carotane index (100 × β–carotane/17α 21β C_{30} hopane) among source rocks with different lithologies. The β-carotane index of mudstone, dolomitic mudstone and argillaceous dolomite range from 0.04 to 0.50 (avg. 0.29), 0.17 to 0.68 (avg. 0.42) and 0.39 to 0.75 (avg. 0.57), respectively (Table 3).

4.4.3. Pentacyclic triterpane

The distribution characteristics of hopanes in source rocks exhibit similarity, with C_{29}-C_{30} hopanes being the predominant compounds and the relative abundance of C_{31} to C_{35} homohopanes decreases progressively (Fig. 4d, e, f). The difference in pentacyclic triterpenes among source rocks with different lithology is primarily reflected in the gammacerane index (gammacerane/17α21βC_{30} hopane). The gammacerane index of mudstone (0.05 to 0.26, avg. 0.15), dolomitic mudstone (0.20 to 0.41, avg. 0.26) and argillaceous dolomite (0.35 to 0.48, avg. 0.41) increased successively (Table 3). The maturity parameters 22S/(22S + 22R) C_{31} hopanes of all samples range from 0.55 to 0.59 (Table 3), are approaching the isomerization equilibrium endpoint.

4.4.4. Steranes

The relative abundance distribution characteristics of C_{27}, C_{28} and C_{29} regular steranes can indicate the source of organic matter (Volkman, 1986; Bechtel et al., 2012). The relative abundance of C_{27}, C_{28} and C_{29} regular steranes in most source rocks of the P_2p shows an increasing trend, with variations observed among source rocks with different

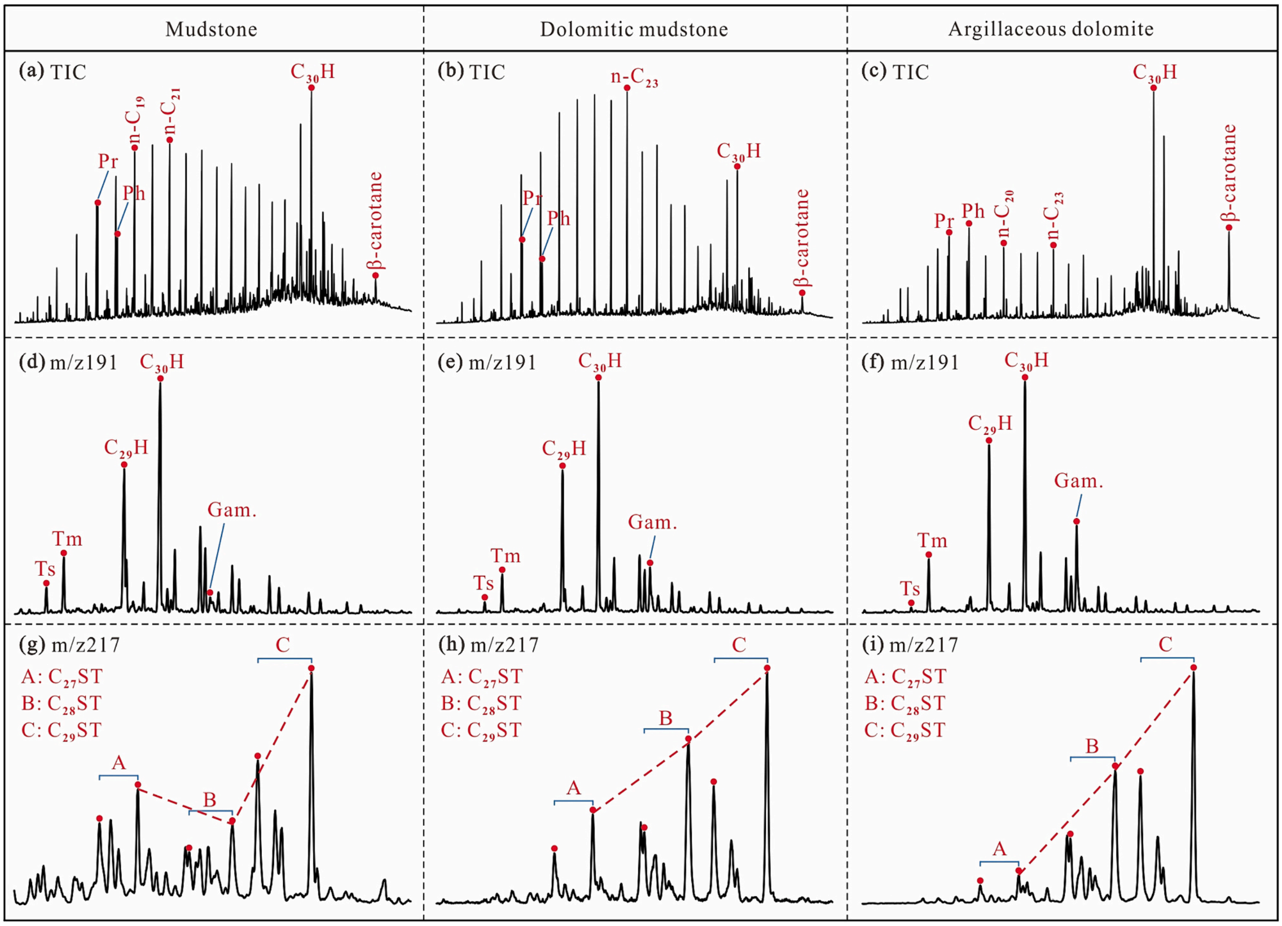

Fig. 4. Gas chromatograms and mass spectrograms of mudstone, dolomite mudstone and argillaceous dolomite of the P_2p, Shishugou Sag, Junggar Basin. Note: Pr = Pristane; Ph = Phytane; Ts = 18α(H),21β(H)-22,29,30-trisnorneohopane; Tm = 17α(H),21β(H)-22,29,30-trisnorhopane; H = Hopane; Gam. = Gammacerane; ST = Sterane.

Table 3
The main parameters of saturated biomarker of source rock samples from the P_2p, Shishugou Sag, Junggar Basin.

Parameters	Mudstone (N = 15)			Dolomitic mudstone (N = 10)			Argillaceous dolomite (N = 5)			All samples (N = 30)		
	Minimum	Maximum	Mean	Minimum	Maximum	Mean	Minimum	Maximum	Mean	Minimum	Maximum	Mean
CPI	1.09	1.48	1.27	1.15	1.33	1.22	1.15	1.47	1.26	1.09	1.48	1.25
$\Sigma nC_{21}^{-}/\Sigma nC_{22}^{+}$	0.60	1.95	1.13	0.69	1.37	1.11	0.78	1.58	1.10	0.60	1.95	1.12
Pr/nC_{17}	0.40	2.80	1.19	0.37	2.20	1.20	1.47	2.93	1.97	0.37	2.93	1.32
Ph/nC_{18}	0.23	2.21	0.94	0.19	2.19	1.00	1.13	2.83	1.65	0.19	2.83	1.08
Pr/Ph	1.04	1.95	1.39	0.95	1.75	1.38	1.21	1.73	1.49	0.95	1.95	1.40
β–carotane index	0.04	0.50	0.29	0.17	0.68	0.42	0.39	0.75	0.57	0.04	0.75	0.38
Gammacerane index	0.05	0.26	0.15	0.20	0.41	0.26	0.35	0.48	0.41	0.05	0.48	0.23
22S/(22S + 22R) C_{31} hopanes	0.55	0.59	0.57	0.57	0.59	0.58	0.57	0.59	0.58	0.55	0.59	0.58
C_{27} regular steranes (%)	16.86	38.10	26.73	9.18	22.87	15.49	5.14	14.35	9.52	5.14	38.10	20.12
C_{28} regular steranes (%)	20.92	38.42	29.59	31.07	42.70	36.95	33.67	42.60	36.66	20.92	42.70	33.22
C_{29} regular steranes (%)	36.99	47.57	43.82	42.45	53.25	47.56	47.79	57.79	53.82	36.99	57.79	46.73
20S/(20S + 20R) C_{29} steranes	0.26	0.50	0.42	0.28	0.47	0.43	0.29	0.48	0.41	0.26	0.50	0.42
ββ/(αα + ββ) C_{29} steranes	0.20	0.42	0.30	0.21	0.42	0.31	0.20	0.37	0.29	0.20	0.42	0.30

"N" is the number of source rock samples. CPI (Scalan and Smith, 1970); β–carotene index = 100 × (β–carotane/17α 21β C_{30} hopane) (Martins et al., 2020); Gammacerane index = gammacerane/17α 21β C_{30} hopane (Moldowan et al., 1985; Sinninghe Damsté et al., 1995); C_{27} regular steranes = $C_{27}/(C_{27} + C_{28} + C_{29})$ regular steranes (%); C_{28} regular steranes = $C_{28}/(C_{27} + C_{28} + C_{29})$ regular steranes (%); C_{29} regular steranes = $C_{29}/(C_{27} + C_{28} + C_{29})$ regular steranes (%).

lithologies. The relative abundance of C_{27} regular steranes decreases successively in mudstone (16.86 to 38.10%, avg. 26.73%), dolomitic mudstone (9.18 to 22.87%, avg. 15.49%) and argillaceous dolomite (5.14 to 14.35%, avg. 9.52%). Conversely, the relative abundance of C_{29} regular steranes increases successively in mudstone (36.99 to 47.57%, avg. 43.82%), dolomitic mudstone (42.45 to 53.25%, avg. 47.56%) and argillaceous dolomite (47.79 to 57.79%, avg. 53.82%) (Table 3). These characteristics suggest that the relative organism composition of source rocks with different lithologies is different. Additionally, the 20S/(20S + 20R) isomerization ratio of C_{29} regular steranes varies between 0.26 and 0.50 (avg. 0.42). The ββ/(ββ + αα) isomerization ratio of the C_{29} regular steranes ranges from 0.20 to 0.42 (avg. 0.30) (Table 3). The maturity parameters mentioned above follow the thermal evolution stage depicted in Fig. 2b.

4.5. Major and trace elements

The major elements, predominantly SiO_2, Al_2O_3, CaO and MgO, constituted a significant proportion in all samples, with an average of 52.84%, 10.85%, 11.85% and 9.27%, respectively (Table 4). It is noteworthy that the content of MgO progressively increased in mudstone, dolomitic mudstone and argillaceous dolomite, with ranges of 2.04 to 8.71% (avg. 4.55), 6.99 to 14.52% (avg. 9.33) and 12.62 to 20.01% (avg. 15.95%), respectively (Table 4). In addition, the ratios of certain trace elements exhibit significant variations among source rocks with different lithologies, encompassing the C value, Sr/Cu, Rb/Sr, Sr/Ba, Li/Al and Cr/Zr ratios. Among these parameters, the C value is defined as C value = $\Sigma(Fe + Mn + Cr + Ni + V + Co)/\Sigma(Ca + Mg + Sr + Ba + K + Na)$ (Zhao et al., 2007; Moradi et al., 2016; Zhang et al., 2020). Compared to dolomitic mudstone and argillaceous dolomite, the mudstone exhibits significantly lower Sr/Cu, Sr/Ba, Li/Al and Cr/Zr ratios while displaying higher C values and Rb/Sr ratios (Table 4). The ratios of certain trace elements display discernible variations among source rocks with different lithologies, suggesting distinct sedimentary environments during their formation.

5. Discussion

5.1. Depositional environment analysis

5.1.1. Palaeoclimate

Sr is known to preferentially accumulate in association with arid conditions whereas Cu is usually concentrated under humid conditions, and Rb is known to be relatively stable during continental weathering whereas Sr is more vulnerable to leaching loss (Lerman and Gat, 1989; Jin and Zhang, 2002; Moradi et al., 2016). Therefore, the Sr/Cu and Rb/Sr ratios are widely employed as indicators of paleoclimate changes in lacustrine sediments due to the sensitivity of elements such as Rb, Sr and Cu to these changes (Lerman, 1978; Sawyer, 1986). Generally, the Sr/Cu ratios are 1.0–5.0, 5.0–10.0 and > 10.0, reflecting warm–humid conditions, semi-arid–humid conditions and arid–hot conditions, respectively (Lerman, 1978; Liu and Zhou, 2007). Higher Rb/Sr ratios indicate a warm-humid palaeoclimate, while lower Rb/Sr ratios indicate an arid-hot palaeoclimate (Bai et al., 2015; Tao et al., 2017). The Sr/Cu ratios of the P_2p mudstone, dolomitic mudstone and argillaceous dolomite range from 0.98 to 7.88 (avg. 4.68), 5.93 to 16.51 (avg. 10.15) and 11.99 to 25.15 (avg. 19.82), respectively (Table 4). Additionally, the Rb/Sr ratios of mudstone (0.20 to 1.78, avg. 0.62), dolomitic mudstone (0.06 to 0.21, avg. 0.12) and argillaceous dolomite (0.02 to 0.13, avg. 0.06) decreased successively (Table 4). This results suggests a transition in paleoclimate from warm-humid conditions to arid-hot conditions during the deposition from mudstone, dolomitic mudstone to argillaceous dolomite (Fig. 5a). Mudstone was deposited under warm-humid or semi-arid humid conditions, dolomitic mudstone was formed in semi-arid humid or arid-hot conditions and argillaceous dolomite was deposited under arid-hot conditions.

The C value is commonly employed as a reliable paleoclimate indicator, as Fe, Mn, Cr, Ni, V and Co are accumulated in a humid environment, while Ca, Mg, Sr, Ba, K and Na are typically enriched under arid conditions (Moradi et al., 2016). The C values of source rocks with different lithologies show distinct variations, as evident from Table 4 and Fig. 5b. Mudstone displays significantly higher C values ranging from 0.22 to 0.46 (avg. 0.31), indicating a semiarid and semiarid to semihumid paleoclimate. Dolomitic mudstone exhibits C values ranging from 0.16 to 0.25 (avg. 0.20), suggesting a semiarid to arid paleoclimate. Notably, argillaceous dolomite shows conspicuously low C values (0.09 to 0.16, avg. 0.13), reflecting that it was deposited in an arid paleoclimate.

The mudstone, dolomitic mudstone and argillaceous dolomite of the P_2p were deposited in different paleoclimate conditions, based on the interpretation of major and trace element by parameters such as C value,

Table 4
The main parameters of major and trace element of source rock samples from the P_2p, Shishugou Sag, Junggar Basin.

Indicative meaning	Parameters	Mudstone (N = 10)			Dolomitic mudstone (N = 9)			Argillaceous dolomite (N = 7)			All samples (N = 26)		
		Minimum	Maximum	Mean	Minimum	Maximum	Mean	Minimum	Maximum	Mean	Minimum	Maximum	Mean
Major oxide	SiO_2 (%)	58.09	69.99	63.36	42.12	58.38	51.52	29.18	44.41	39.51	29.18	69.99	52.84
	Al_2O_3 (%)	9.43	16.10	12.73	8.45	12.69	10.50	6.81	11.93	8.60	6.81	16.10	10.85
	CaO (%)	0.98	6.81	3.97	8.43	20.26	13.14	18.30	27.61	21.44	0.98	27.61	11.85
	MgO (%)	2.04	8.71	4.55	6.99	14.52	9.33	12.62	20.01	15.95	2.04	20.01	9.27
Paleoclimate	C-value	0.22	0.46	0.31	0.16	0.25	0.20	0.09	0.16	0.13	0.09	0.46	0.22
	Sr/Cu	0.98	7.88	4.68	5.93	16.51	10.15	11.99	25.15	18.82	0.98	25.15	10.38
	Rb/Sr	0.20	1.78	0.62	0.06	0.21	0.12	0.02	0.13	0.06	0.02	1.78	0.30
Paleosalinity	Sr/Ba	0.26	0.87	0.60	0.85	1.98	1.40	1.84	3.07	2.38	0.26	3.07	1.35
Redox conditions	Mo_{EF}	2.61	8.36	5.81	2.36	15.13	7.62	1.99	8.03	4.74	1.99	15.13	6.15
	U_{EF}	0.72	1.84	1.19	0.92	2.92	1.99	0.72	4.26	1.95	0.72	4.26	1.67
	δU	1.47	1.77	1.60	1.43	1.82	1.70	1.47	1.83	1.62	1.43	1.83	1.64
	V/(V + Ni)	0.70	0.85	0.79	0.73	0.88	0.80	0.69	0.86	0.77	0.69	0.88	0.79
Paleoproductivity	Cu/Al	4.60	16.36	10.33	6.60	17.75	11.00	5.36	19.09	11.88	4.60	19.09	10.98
	Ni/Al	2.56	6.93	5.20	3.87	6.70	5.11	3.22	7.14	5.17	2.56	7.14	5.16
	Zn/Al	9.58	35.90	19.82	8.11	34.80	17.85	9.60	27.94	18.60	8.11	35.90	18.81
Volcanic ash input	Zr/Al_2O_3	7.29	22.56	12.68	4.44	20.51	11.43	5.90	22.20	13.07	4.44	22.56	12.35
Hydrothermal activity	Li/Al	3.33	29.65	14.41	13.59	41.38	27.14	26.38	54.60	38.60	3.33	54.60	25.33
	Cr/Zr	0.07	0.33	0.22	0.13	0.41	0.25	0.29	0.51	0.41	0.07	0.51	0.28

"N" is the number of source rock samples.

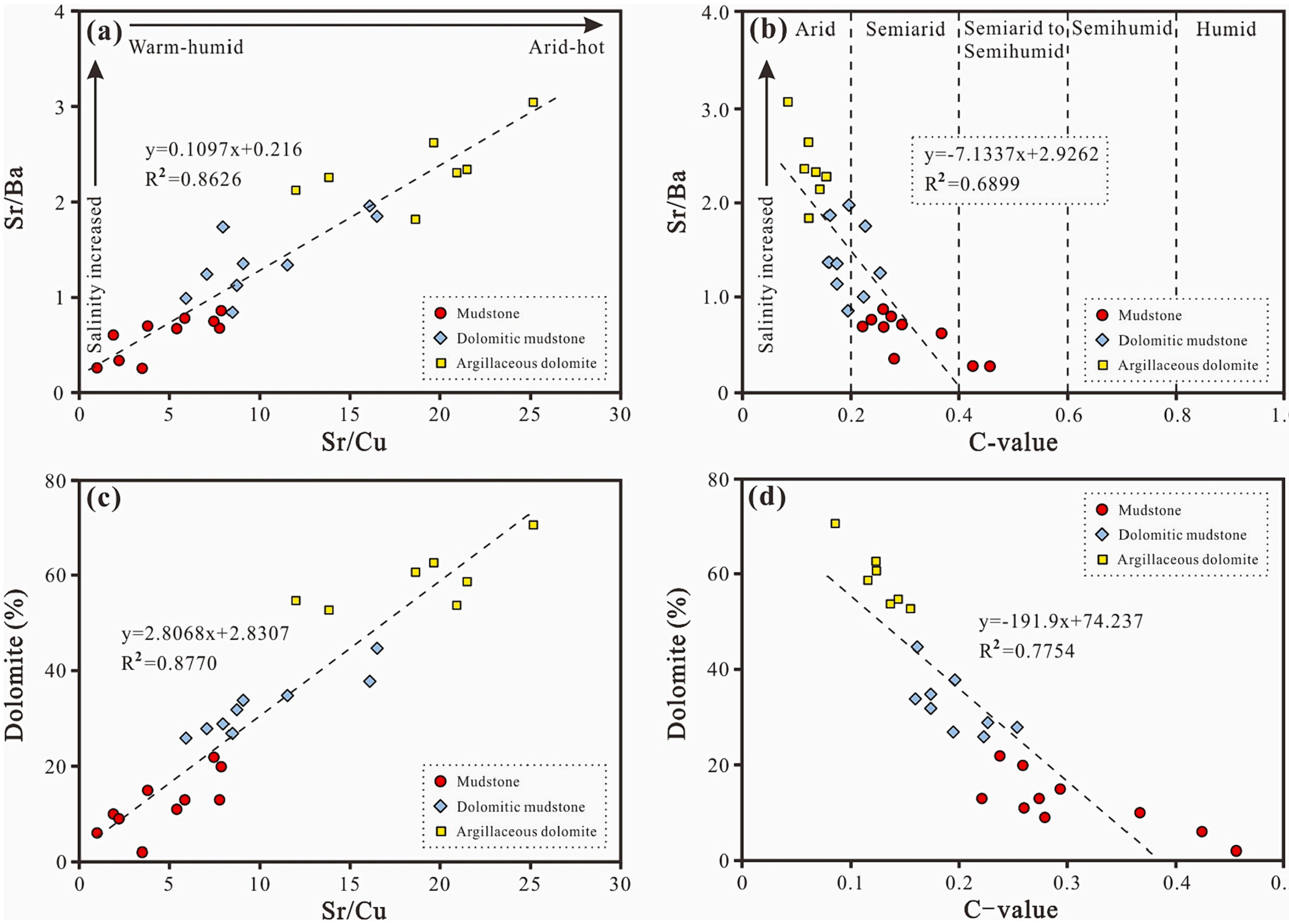

Fig. 5. (a-b) The crossplots of paleoclimate parameters (Sr/Cu; C-value) versus Sr/Ba ratios of source rock samples from the P_2p, Shishugou Sag, Junggar Basin; (c-d) The crossplots of paleoclimate parameters (Sr/Cu; C-value) versus dolomite content of source rock samples from the P_2p, Shishugou Sag, Junggar Basin.

Sr/Cu and Rb/Sr ratio. In addition, the influence of paleoclimate conditions on dolomite formation in the mixed sedimentary rocks of the P_2p can be observed from Fig. 5c and d. An increased dolomite content is associated with decreased C value and increased Sr/Cu ratio in source rocks, suggesting that arid paleoclimate conditions promote dolomite precipitation (Fig. 5c, d). The main reason is that the evaporation gradually enhances during the paleoclimate transition towards arid-hot conditions, increasing Mg^{2+} concentration and Mg/Ca ratio. This facilitates the creation of a suitable water environment for dolomite formation (Machel, 2004; Manche and Kaczmarek, 2019, 2021). Additionally, frequent hydrothermal and microbial activities within the study area disrupt the robust hydrated shell surrounding Mg^{2+} ions and facilitate dolomite formation (Slaughter and Hill, 1991; Kenward et al., 2009; Perri et al., 2018; Sun et al., 2021). Consequently, hydrothermal and microbial activities disrupt the thermodynamic barrier to dolomite formation, while the periodic fluctuations in paleoclimate play a crucial role in controlling dolomite deposition, resulting in the interbedded deposition of mudstone, dolomitic mudstone and argillaceous dolomite.

5.1.2. Paleosalinity

The salinity in lacustrine systems often influences the stratification of the water column and redox conditions, which play a pivotal role in the preservation of organic matter following organismal death (Eugster and Hardie, 1978; Wei et al., 2018; Pan et al., 2020). The high abundance of gammacerane indicates saline water and stratification of the water column (Moldowan et al., 1985; Sinninghe Damsté et al., 1995; Liu et al., 2017; Martins et al., 2020). The presence of β-carotene is typically observed in sediments formed under reducing and saline water conditions due to their sensitivity to oxygen (Murphy et al., 1967; Moldowan et al., 1985; Requejo et al., 1992; Ding et al., 2017; Xia et al., 2021). Therefore, the gammacerane index and β-carotene index can effectively indicate the salinity variations in the water column. The sequential increase in the gammacerane index and β-carotene index of mudstone, dolomitic mudstone and argillaceous dolomite suggests a progressive rise in water salinity during their sedimentary periods (Table 3, Fig. 6a).

The Sr/Ba ratio serves as a reliable indicator for assessing paleosalinity. Generally, a low Sr/Ba ratio (< 0.6) is indicative of fresh water, an intermediate Sr/Ba ratio (0.6 to 1.0) suggests brackish water and a high Sr/Ba ratio (> 1.0) indicates salt water (Rohling, 2000; Zhang et al., 2018; Wei and Algeo, 2020). The Sr/Ba ratios of the P_2p mudstone, dolomitic mudstone and argillaceous dolomite increase successively (Fig. 5a, b), which are 0.26 to 0.87 (avg. 0.60), 0.85 to 1.98 (avg. 1.40) and 1.84 to 3.07 (avg. 2.38), respectively (Table 4). The above data suggest that mudstone was deposited in fresh water to brackish water environments, dolomitic mudstone was deposited in brackish water to salt water environments and argillaceous dolomite was formed in salt water environments. Furthermore, as illustrated in Fig.5a and b, the Sr/Ba ratio in source rocks demonstrates an upward trend with decreasing C value and increasing Sr/Cu ratio, suggesting that paleoclimate conditions primarily control variations in the salinity of the water column.

5.1.3. Redox conditions

The oxidative decomposition of organic matter is prevalent in lake water and sediments; thus, the anoxic environment plays a crucial role

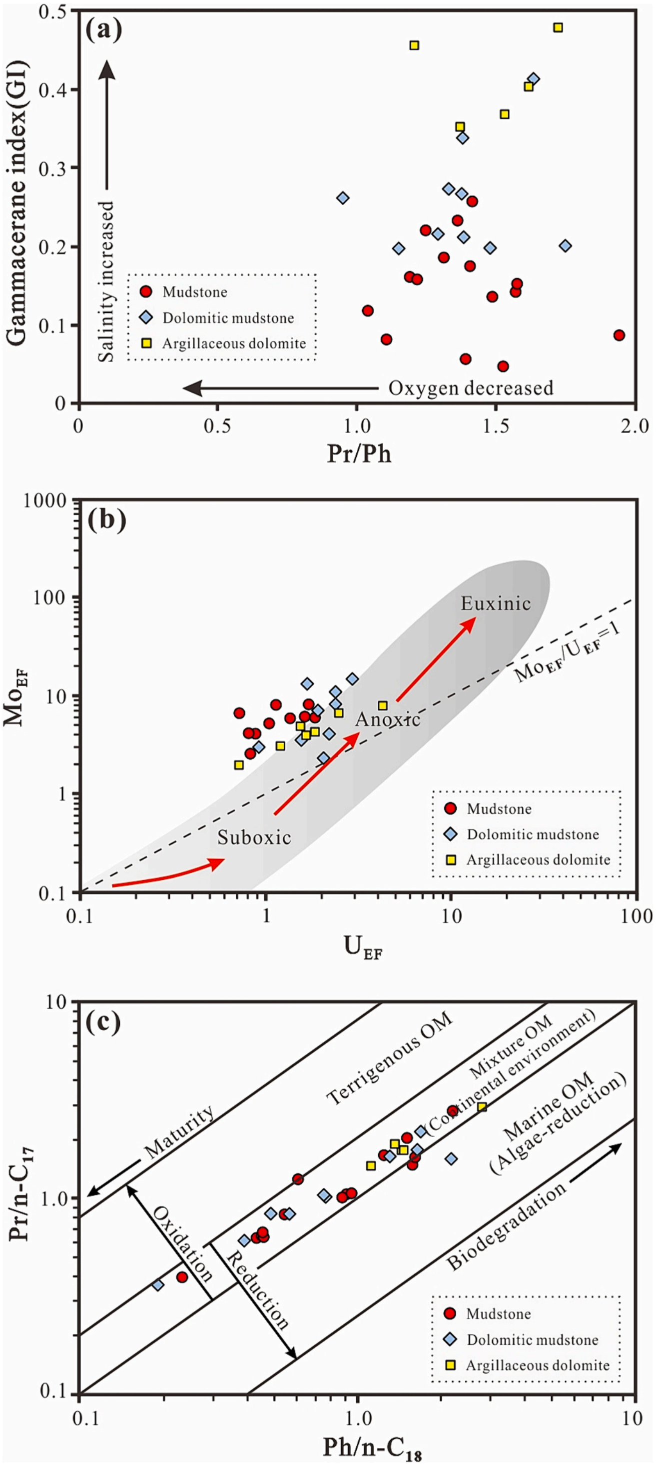

Fig. 6. The crossplots reflecting the Paleosalinity and redox conditions of source rock samples from the P_2p, Shishugou Sag, Junggar Basin. (a) Gammacerane index (GI) versus Pr/Ph; (b) Mo_{EF} versus U_{EF} (modified from Algeo and Tribovillard, 2009); (c) Pr/n-C_{17} versus Ph/n-C_{18} (according to Connan and Cassou, 1980).

in the preservation of organic matter, thereby significantly facilitating the formation of organic-rich source rocks (Demaison and Moore, 1980; Hedges and Keil, 1995; Lash and Blood, 2014; Wang et al., 2017). Currently, some elemental parameters (e.g., U_{EF}, Mo_{EF}, δU, V/(V + Ni)) and biomarker parameters (e.g., Pr/Ph, Pr/nC_{17}, Ph/nC_{18}) are extensively employed for assessing the redox conditions of lake water (Didyk et al., 1978; Tribovillard et al., 2006; Algeo and Liu, 2020).

The enrichment factor is calculated as $X_{EF} = [(X/Al)_{sample}/(X/Al)_{standard}]$, utilizing concentrations of the element of interest and Al in the sample, normalized to the same ratio for a standard shale (e.g., NASC, PAAS) or continental crust (Tribovillard et al., 2006; Algeo and Tribovillard, 2009; Algeo and Liu, 2020). The crossplot of U_{EF} vs. Mo_{EF} in Fig. 6b reveals that the mixed sedimentary rocks of the P_2p predominantly deposited under anoxic water column conditions, and the redox conditions of source rocks with different lithologies exhibit no significant variations. In addition, The δU values are determined using the formula δU = 2 U/(U + Th/3). δU <1.0 and δU > 1.0 reflect aerobic and anoxic conditions, respectively (Steiner et al., 2001). V/(V + Ni) ratios ≤0.46, >0.46 to ≤0.60, >0.60 to ≤0.82, >0.82 correspond to oxic, dysoxic, suboxic to anoxic and euxinic conditions respectively (Hatch and Leventhal, 1992; Jones and Manning, 1994). δU values and V/(V + Ni) of the P_2p mixed sedimentary rocks range from 1.43 to 1.83 (avg. 1.64) and 0.69 to 0.88 (avg. 0.79), respectively (Table 4), representing a suboxic to anoxic conditions.

The interconversion of pristane and phytane bioprecursors under various redox conditions suggests that the Pr/Ph ratio can serve as a reliable indicator for assessing redox conditions (Didyk et al., 1978; ten Haven et al., 1987). Pr/Ph ratio < 0.8 and > 3.0 reflect typical anoxic and oxic conditions, respectively (Didyk et al., 1978; ten Haven et al., 1987; Peters et al., 2005). The Pr/Ph ratios of the P_2p mixed sedimentary rocks range from 0.95 to 1.95 (avg. 1.40) (Table 3), indicating suboxic to anoxic conditions. This finding is consistent with that observed in the crossplot of Pr/nC_{17} vs. Ph/nC_{18} (Fig. 6c). Generally, the Pr/Ph ratio may be affected by organic matter sources and thermal maturity. Considering that the P_2p source rocks primarily consist of algae as the organic matter source with relatively low thermal maturity, the impact of these two factors on Pr/Ph ratio is expected to be limited. However, it is still necessary to integrate both organic and element geochemical indicators to accurately assess the redox conditions of P_2p source rocks.

In conclusion, the mudstone, dolomitic mudstone and argillaceous dolomite of the P_2p in the study area were deposited under suboxic to anoxic conditions. There were no significant variations in redox conditions among the source rocks with different lithologies (Fig. 6a, b, c; Table 4). In saline lacustrine basins, the presence of stratified water columns with higher salinity typically facilitates the formation of anoxic bottom water conditions, which is consistent with the Paleogene Xingouzui Formation in Jianghan Basin (Li et al., 2021), the Middle Permian Lucaogou Formation in Jimsar Sag and Santanghu Basin (Zhang et al., 2019a; Liu et al., 2018; Pan et al., 2021).

5.2. Paleoproductivity and source of organic matter

5.2.1. Paleoproductivity

The elements Cu, Ni and Zn in sediments are typically found within living organisms, forming complexes with organic matter and subsequently precipitating to the bottom of lake water (Martin and Knauer, 1973; Piper and Perkins, 2004; Tribovillard et al., 2006). Consequently, these trace elements have been extensively applied in paleoproductivity assessment (Tribovillard et al., 2006). Elemental ratios (Cu/Al, Ni/Al and Zn/Al) are commonly employed for evaluating the paleoproductivity of source rocks during deposition (Algeo and Maynard, 2004; Shen et al., 2015). Higher ratios of Cu/Al, Ni/Al and Zn/Al indicate greater paleoproductivity (Algeo and Maynard, 2004; Schoepfer et al., 2015).

The Cu/Al, Ni/Al and Zn/Al ratios of the mixed sedimentary rocks from the P_2p in the study area range from 4.60 to 19.09 (avg. 10.98), 2.56 to 7.14 (avg. 5.16) and 8.11 to 35.90 (avg. 18.81), respectively (Table 4). The comparison of Cu/Al values (avg. 3.11), Ni/Al values (avg. 5.48) and Zn/Al values (avg. 8.84) with post-Archean Australian shale indicate a higher paleoproductivity in the P_2p source rocks (Taylor and McLennan, 1985; McLennan, 1989). Furthermore, no significant difference is observed in the average paleoproductivity parameters (Cu/

Al, Ni/Al and Zn/Al) among mudstone, dolomitic mudstone and argillaceous dolomite (Table 4), suggesting that overall paleoproductivity was relatively high across source rocks with different lithologies during the deposition period.

5.2.2. Source of organic matter

The organic matter in terrestrial lake basins primarily originates from terrigenous higher plants and aquatic organisms. Both depositional environment and paleoproductivity have essential effects on the biological source and composition of organic matter (Hao et al., 2011; Song et al., 2019). Typically, organic maceral and biomarker parameters are employed for determining the source of organic matter in source rocks (Seifert and Moldowan, 1978; Philp and Gilbert, 1986; Hackley et al., 2016). The results of organic maceral analysis can intuitively determine the relative proportions of algal and terrigenous organic matter input. The organic maceral of the P_2p mixed sedimentary rocks primarily consists of algae, indicating their significant contribution to organic matter input. The relatively low proportion of terrigenous OM (sporinite, vitrinite and inertinite) in the organic maceral suggests that terrestrial higher plants are not the primary contributors to organic matter (Table 2; Fig. 3).

The P_2p source rocks are currently in low maturation and maturity. Therefore, the distribution characteristics of n-alkanes can effectively indicate the source of organic matter (Cranwell, 1977; Brassell et al., 1978; Wang et al., 2019). Based on the distribution characteristics of n-alkanes, nC_{21}^{-}/nC_{22}^{+} and Pr/nC_{17} vs. Ph/nC_{18}, the organic matter sources of P_2p source rocks are mainly aquatic organisms, followed by terrigenous higher plants.

Regular steranes are commonly used to indicate the biological origin of sedimentary organic matter (Huang and Meinschein, 1979; Bechtel et al., 2012). C_{27} regular steranes are typically derived from aquatic organisms such as zooplankton and algae (Huang and Meinschein, 1979). C_{28} regular steranes indicate the origin of planktonic organisms that contain chlorophyll *c*, such as diatoms and cyanobacteria (Grantham and Wakefield, 1988; Liu et al., 2022). The findings of this study suggest that the C_{28} regular steranes present in the mixed sedimentary rocks of the P_2p within the study area are primarily derived from cyanobacteria. Firstly, extensive cultivation of modern cyanobacteria in a glucose culture medium revealed a substantial production of ergosterol (1033.3 μg/g), a biological precursor to C_{28} regular sterane (Fagundes et al., 2019). Secondly, current research indicates that diatoms emerged during the Jurassic or Cretaceous period, with a significant temporal gap from the Permian era, whereas cyanobacteria have been present since the Cambrian period (Grantham and Wakefield, 1988). Therefore, it is more likely that the source of C_{28} regular steranes in the P_2p source rocks is cyanobacteria rather than diatoms.

C_{29} regular steranes indicate a source from terrigenous higher plants (Volkman, 1986). However, recent studies have shown that C_{29} regular steranes can also originate from certain microalgae species, such as green algae (Volkman et al., 1998; Ding et al., 2019). This study suggests that the C_{29} regular steranes found in the mixed sedimentary rocks of the P_2p primarily originate from green algae rather than terrigenous higher plants. The following reasons support this conclusion: Firstly if the abundant C_{29} regular steranes were derived from terrigenous higher plants, it contradicts the predominance of type I-II$_1$ organic matter (Fig. 2b). Secondly, a lower content of terrigenous OM in organic macerals and a reduced abundance of long-chain n-alkanes (n-C_{27-31}) in biomarkers indicate a lesser contribution from terrigenous higher plants. Thirdly, previous studies have demonstrated the absence of terrigenous higher plants in certain basins within the United States Ordovician source rocks (Ryder et al., 1998). Nevertheless, these source rocks contain a high abundance of C_{29} regular steranes derived from extensively developed green algae and dinoflagellates during that period (Ryder et al., 1998). During the sedimentary period of the P_2p mixed sedimentary rocks, green algae thrived while dinoflagellates were scarce. Additionally, C_{29} regular steranes were abundant in the source rocks, similar to the above case observed in certain Ordovician basins within the United States (Grantham and Wakefield, 1988).

Previous studies based on organic petrology, molecular geochemistry, element geochemistry and isotopic composition analysis of source rock have demonstrated that the C_{28} regular steranes and C_{29} regular steranes present in the Lucaogou Formation's source rocks within Jimusar Sag were primarily derived from cyanobacteria and green algae, respectively (Fu et al., 1990; Xia et al., 2021; Liu et al., 2022; Zhi et al., 2023; Zeng et al., 2023b). Therefore, based on the above analysis, this study concludes that the C_{28} regular steranes in the mixed sedimentary rocks of the P_2p within the study area predominantly originate from cyanobacteria, while the C_{29} regular steranes primarily derive from green algae. Further analysis of Fig. 7 reveals a significant correlation between the relative abundance of regular steranes and the gammacerane index, suggesting that variations in water column salinity can substantially influence the biological composition of endogenous organic matter. Fig. 7a and b demonstrate that salt-intolerant algae and salt-tolerant green algae provide the bioprecursors of C_{27} and C_{29} regular steranes, respectively. The abundance of C_{28} regular steranes initially increased and then decreased with the increase of the gammacerane index (Fig. 7c), primarily due to the slight salt tolerance of cyanobacteria (Warren, 2016). High salinity water can disrupt ion balance inside and outside cyanobacterial cells, affecting their physiological metabolism and limiting growth and development (Singh et al., 2022).

Consequently, the salinity increased in the water column as the paleoclimate tended to be increasingly arid (Fig. 6a, b), reducing the proportion of salt-intolerant algae (primarily contributing to bioprecursors of C_{27} regular steranes) within endogenous organic matter (Fig. 7a). Conversely, there is an elevation in the proportion of slightly salt-tolerant cyanobacteria (mainly provide bioprecursors for C_{28} regular steranes) and salt-tolerant green algae (mainly provide bioprecursors for C_{29} regular steranes) within endogenous organic matter (Fig. 7b, c). Moreover, the arid paleoclimate facilitates dolomite formation and promotes the deposition of dolomitic mudstone and argillaceous dolomite. As a result, the abundance of C_{27} regular steranes in dolomitic mudstone and argillaceous dolomite is comparatively lower than that in mudstone, while the abundance of C_{28} and C_{29} regular steranes is relatively higher (Fig. 7).

5.3. Hydrothermal activity

Microscopic thin section identification and electron probe analysis have confirmed the influence of hydrothermal activities on the deposition of the P_2p source rocks (Fan et al., 2021). Additionally, the ternary diagram of trace elements demonstrates that the mixed sedimentary rocks of the P_2p are situated within a hydrothermal deposition zone (Fig. 8a, b), suggesting a significant involvement of hydrothermal fluids in the depositional processes of source rocks.

Previous studies have demonstrated that the enrichment of Mn and certain incompatible elements (e.g., Li) are indicators of significant hydrothermal influence (Pisarskii et al., 1998; Balistrieri et al., 2007), and Pierret et al. (2000) demonstrated the utility of the Cr vs. Zr ratio to detect hydrothermal influence. Therefore, the Li/Al and Cr/Zr ratios can indicate the intensity of hydrothermal activity, with higher values reflecting stronger hydrothermal activity (Marchig et al., 1982; Pisarskii et al., 1998; Pujol et al., 2006; Tao et al., 2022). The Li/Al ratios of the P_2p mudstone, dolomitic mudstone and argillaceous dolomite are 3.33 to 29.65 (avg. 14.41), 13.59 to 41.38 (avg. 27.14), 26.38 to 54.60 (avg. 38.60), respectively (Table 4). The ratios of Cr/Zr are 0.07 to 0.33 (avg. 0.22), 0.13 to 0.41 (avg. 0.25) and 0.29 to 0.51 (avg. 0.41), respectively (Table 4). These data show that the intensity of hydrothermal activity increases gradually during the sedimentary period from mudstone, dolomitic mudstone to argillaceous dolomite. Additionally, the content of Mg^{2+} in mudstone, dolomitic mudstone and argillaceous dolomite increases with the enhancement of hydrothermal activity (Fig. 9a, b), indicating that the hydrothermal fluid rich in Mg ions plays a role in the

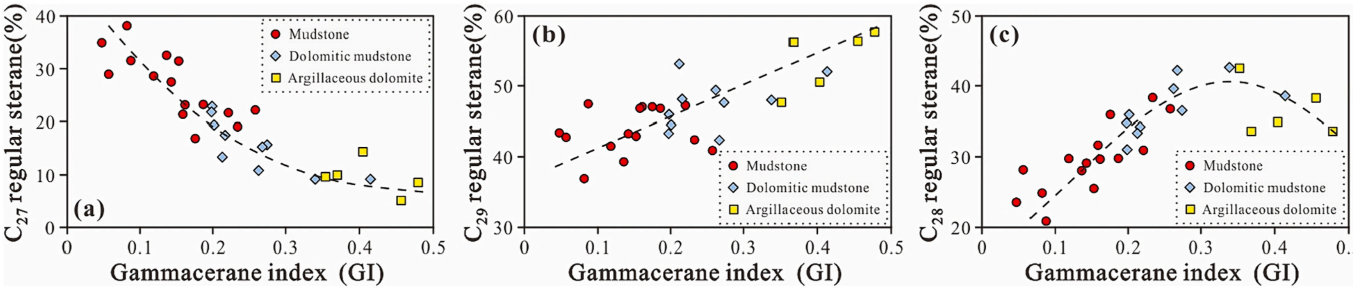

Fig. 7. The crossplots of regular steranes (C_{27}–C_{29}) versus gammacerane index (GI) of source rock samples from the P_2p, Shishugou Sag, Junggar Basin.

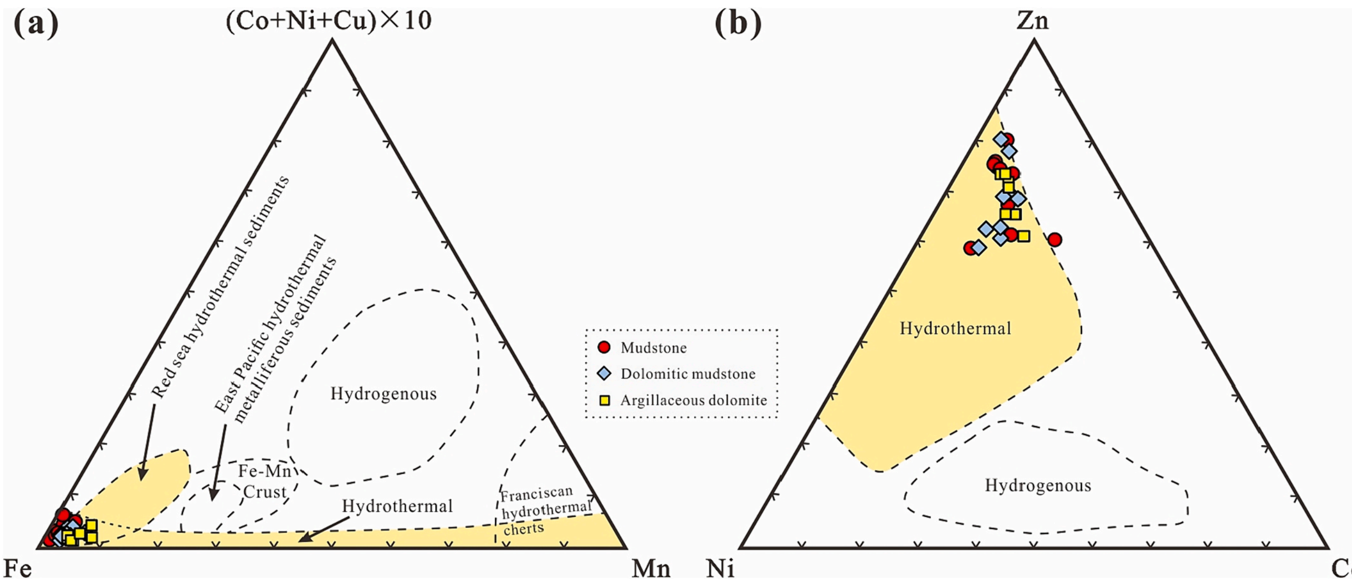

Fig. 8. (a) Ternary plot of Fe vs. Mn vs. (Cu + Co + Ni) × 10 after Crerar et al., 1982. (b) Ternary plot of Ni vs. Co vs. Zn after Choi and Hariya, 1992.

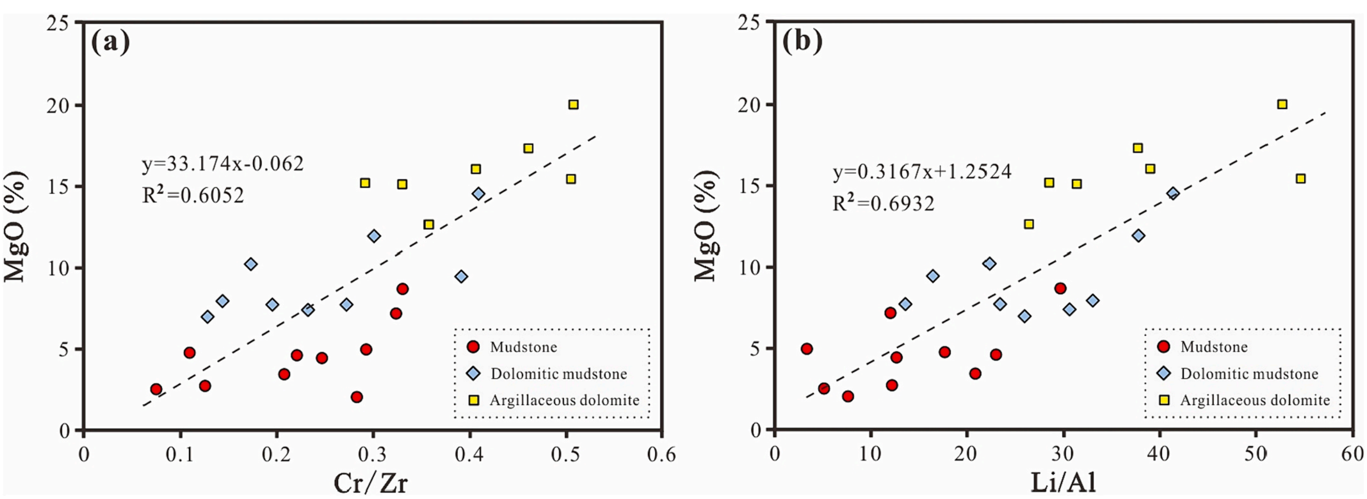

Fig. 9. The crossplots reflect the influence of hydrothermal activity (a: Cr/Zr versus MgO; b: Li/Al versus MgO) on the source of magnesium.

increase of Mg^{2+} concentration in the lake water (Kenward et al., 2009). During the P_2p sedimentary period, significant hydrothermal fluids containing Mg^{2+} infiltrated the lake through faults or fractures, providing a plentiful source of Mg ions for dolomite formation. Moreover, the evaporation of lake water resulting from a relatively arid paleoclimate and the metabolic activities of microorganisms such as bacteria can facilitate an elevation in the concentration of Mg^{2+}.

5.4. Influencing factors of organic matter enrichment

The organic matter enrichment in basins is generally influenced by multiple factors, particularly paleoproductivity and redox conditions (Pedersen and Calvert, 1990; Calvert and Pedersen, 1993; Bohacs et al., 2005; Katz, 2005; Lash and Blood, 2014; Wu et al., 2019; Wang et al., 2021). In the study area, there is no apparent correlation between TOC and paleoclimate parameters (C-value, Sr/Cu and Rb/Sr), paleosalinity parameters (Sr/Ba and Gammacerane index), or redox condition parameters (Pr/Ph, δU and V/(V + Ni)) in the P_2p source rocks (Fig. 10). Nevertheless, this does not imply that the depositional environment has no impact on organic matter accumulation in the mixed sedimentary rocks of the P_2p. The reason is that the saline, stratified and anoxic water column during the sedimentary period of the source rocks was caused by relatively arid paleoclimate, which was conducive to the preservation of organic matter.

The weak correlation between regular sterane (C_{27}, C_{28} and C_{29} regular sterane) and TOC, as depicted in Fig. 11a, b and c, suggests that the relative proportions of salt-tolerant algae, slightly salt-tolerant cyanobacteria and salt-tolerant green algae do not significantly influence the enrichment of organic matter. However, there was a significant positive correlation between TOC and endogenous/terrigenous OM (R^2 = 0.6985, *p*-value =0.23) (Fig. 11d), indicating that an increase in the contribution of algal organic matter compared to terrigenous higher plants can enhance the organic matter abundance and consequently promote organic matter enrichment in source rocks.

Furthermore, a good positive correlation between TOC and paleoproductivity indicators (Cu/Al, Ni/Al and Zn/Al ratios) suggests that the organic matter enrichment in the mixed sedimentary rocks of the P_2p is primarily governed by paleoproductivity, which was influenced by extensive volcanic activity during the Permian period in the Junggar Basin (Fig. 11e, f, g) (Zhang et al., 2015; Ding et al., 2020; Meng et al., 2022). Previous studies through thin section observations have demonstrated that the Middle Permian source rocks in the eastern Junggar Basin generally contain tuffaceous materials, indicating their deposition process was influenced by volcanic activities (Jiang et al., 2015; Ding et al., 2019; Meng et al., 2022). In addition, Zr/Al_2O_3 can serve as an effective geochemical indicator for assessing the input of volcanic ash in lacustrine source rocks (Suzuki et al., 1998; Pujol et al., 2006; Yang et al., 2022). A clear positive correlation between TOC and Zr/Al_2O_3 suggests that the influx of volcanic ash enhanced paleoproductivity in the mixed sedimentary rocks of the P_2p (Fig. 11h).

Frequent volcanic activity facilitates the influx of Cu, Ni, Zn and other nutrients from volcanic ash into the lake, stimulating algal bloom and enhancing paleoproductivity (Langmann et al., 2010; Olgun et al., 2013). Conversely, during periods of intermittent volcanic activity, nutrient input decreases and restricts algal growth, resulting in low paleoproductivity. Hence, volcanic activity is crucial in influencing paleoproductivity and controlling the organic matter enrichment in the mixed sedimentary rocks. Additionally, the weak correlation observed between the hydrothermal activity parameters (Cr/Zr and Li/Al ratios) and TOC suggests that the intensity of hydrothermal activity is not the primary factor affecting organic matter enrichment of the P_2p source rocks in this study area (Fig. 11i, j).

5.5. *Formation mechanism of organic-rich mixed sedimentary rocks*

Based on the analysis above, the formation mechanism of organic-rich mixed sedimentary rocks in the study area is intricate and

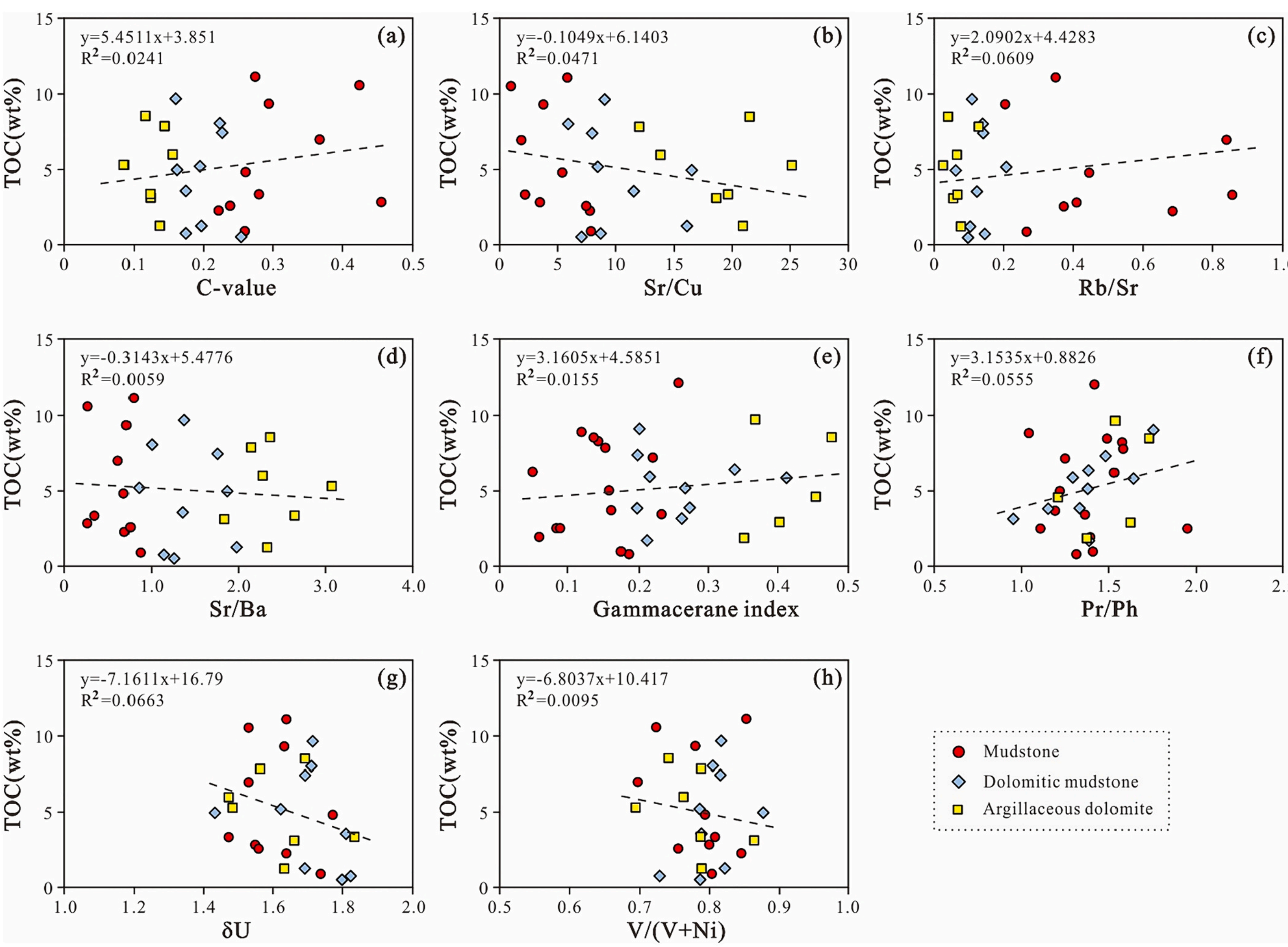

Fig. 10. The correlation between TOC and paleoclimate parameter (a–c: C-value, Sr/Cu, Rb/Sr), paleosalinity parameter (d–e: Sr/Ba, Gammacerane index) and redox indicators (f–h: Pr/Ph, δU, V/(V + Ni)) of source rock samples from the P_2p, Shishugou Sag, Junggar Basin.

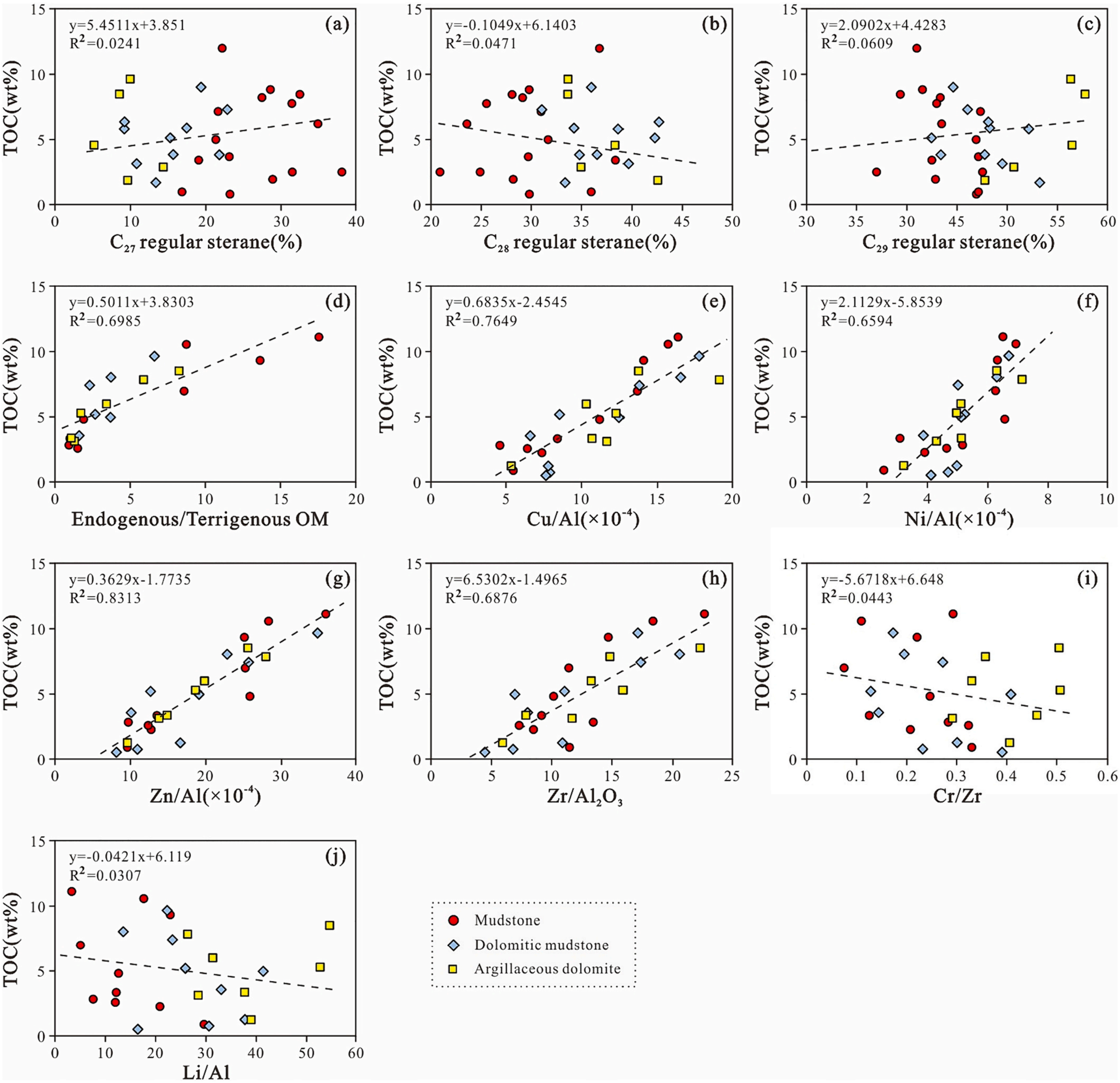

Fig. 11. The correlation between TOC and organic matter origin parameters (a–c: C_{27}, C_{28}, C_{29} regular sterane; d: alginate/terrigenous OM), primary productivity parameters (e–g: Cu/Al, Ni/Al, Zn/Al), Volcanic ash input parameter (h: Zr/Al_2O_3) and hydrothermal activity parameters (i–j: Cr/Zr, Li/Al) of source rock samples from the P_2p, Shishugou Sag, Junggar Basin.

influenced by factors such as paleoenvironment, paleoproductivity, volcanic activity and hydrothermal activity. The mixed sedimentary rocks of the P_2p were deposited in a relatively stable saline lacustrine environment, thereby creating favorable conditions for the development of organic-rich source rocks. During the P_2p deposition period, there are apparent differences in the sedimentary environment among mudstone, dolomitic mudstone and argillaceous dolomite. Compared to dolomitic mudstone and argillaceous dolomite, the paleoclimate during mudstone deposition was more humid with weaker evaporation. Consequently, this resulted in lower concentrations of Mg^{2+} in lake water that hindered dolomite formation and ultimately led to low dolomite content in mudstone.

Conversely, during deposition periods of dolomitic mudstone and argillaceous dolomite, paleoclimate conditions become increasingly arid with enhanced evaporation, leading to higher concentrations of Mg^{2+}. Additionally, the hydrothermal fluid transports mantle-derived material into the lake, where abundant input of Mg^{2+} combined with arid paleoclimate facilitated extensive dolomite precipitation, forming dolomitic mudstone and argillaceous dolomite. Therefore, paleoclimate and hydrothermal activities jointly promoted the interbedded deposition of the P_2p mixed sedimentary rocks with different lithologies in the saline lake basin. Frequent hydrothermal activities result in a persistent presence of Mg^{2+} in the lake. During arid and hot paleoclimates, the concentration of Mg^{2+} increases due to evaporation, thereby facilitating dolomite formation. Conversely, during warm and humid paleoclimates, the lake exhibits a relatively low concentration of Mg^{2+}, which impeded extensive dolomite precipitation.

Additionally, as paleoclimate conditions progressively became more arid, the salinity of the water column in the lake basin gradually increased(Fig. 5a, b), exerting a significant influence on changes in algae species within endogenous organic matter. The salinity increase in the water column resulted in a higher proportion of salt-tolerant green algae and slightly more salt-tolerant cyanobacteria than salt-intolerant algae. As a result, the proportion of organic matter input from salt-intolerant algae is lower in dolomitic mudstone and argillaceous dolomite compared to mudstone. Generally, saltwater environments can decrease the proportion of salt-intolerant algae, resulting in reduced biodiversity in saline lake basins. However, a reduction in biodiversity does not necessarily result in a decline in the total biomass. This is because salt-tolerant algae, such as cyanobacteria and green algae, can adapt to survive in saline water environments and replace salt-intolerant algae through interspecific competition (Warren, 2016; Xia et al., 2021).

During the deposition of the P_2p, volcanic activity positively influenced the formation of organic-rich mixed sedimentary rocks. In general, an appropriate influx of volcanic material can trigger rapid biological development and play a crucial role in forming high-quality source rocks (Langmann et al., 2010; Olgun et al., 2013). The frequent volcanic eruptions during the Permian period in the Junggar Basin resulted in the transportation of volcanic materials by wind into the lake, bringing a large amount of nutrients and establishing a rich foundation for the formation of high-quality source rocks. The correlation between TOC and volcanic activity, as well as paleoproductivity parameters (Fig. 11e, f, g, h), demonstrates that increased paleoproductivity caused by volcanic activity is the primary factor contributing to organic matter enrichment in the mixed sedimentary rocks within the study area. Furthermore, stratification of the water column commonly occurs in saline lake basins, thereby creating a stable anoxic environment that facilitates the preservation of organic matter, which can also promote the enrichment of organic matter in source rocks.

In conclusion, the formation of mixed sedimentary rocks in the study area is influenced by paleoenvironmental conditions, paleoproductivity, volcanic activity and hydrothermal activity. The dynamic changes in paleoclimate and hydrothermal activity control the development of source rocks with different lithologies, resulting in interbedded deposition of mudstone, dolomitic mudstone and argillaceous dolomite. Fluctuations in salinity caused by paleoclimate are primarily responsible for differences in the proportion of salt-tolerant and salt-intolerant algae within source rocks of different lithologies. Enhanced paleoproductivity caused by volcanic activity is crucial in promoting organic matter accumulation within these mixed sedimentary rocks.

5.6. Implications

Taking the Pingdiquan Formation in Shishugou Sag, Junggar Basin as a case study, this paper elucidates the differences in geochemical characteristics and formation mechanisms of mixed sedimentary rocks within continental saline lacustrine basins. These findings have some significant implications for future exploration and development endeavors, as well as fundamental research undertakings: (1) The different sedimentary environments of mudstone, dolomitic mudstone and argillaceous dolomite, result in significant variations in biomarker parameters, including the gammacerane index, β-carotene index and regular sterane parameters. The combination of these parameters provides a crucial foundation for classifying crude oil types and oil source correlation within the study area. (2) The proportions of salt-tolerant and salt-intolerant algae in mixed sedimentary rocks vary under different salinity conditions. Therefore, further research can focus on conducting a comparative analysis of hydrocarbon generation evolution characteristics within mixed sedimentary rocks where salt-tolerant algae and salt-intolerant algae serve as the primary source of organic matter, respectively. Moreover, it is also essential to analyze the impacts of algal species variation on the oil-generation potential of source rocks during various hydrocarbon generation stages. (3) Generally, halocline commonly occurs in continental saline lake basins, leading to the stratification of water columns and an anoxic bottom water environment that favors organic matter preservation. Consequently, the abundance of organic matter in source rocks varies significantly among different continental saline lake basins, with paleoproductivity differences likely serving as the decisive factor.

6. Conclusions

(1) The P_2p in the Shishugou Sag contains mixed sedimentary rocks, including mudstone, dolomitic mudstone and argillaceous dolomite, which exhibit high hydrocarbon generation potential and can serve as source rocks rich in organic matter.
(2) The frequently changing paleoclimate and hydrothermal activity controls the formation of source rocks with different lithologies. During the sedimentary period of the P_2p, Mg^{2+} was supplied through frequent hydrothermal activities. Moreover, Mg^{2+} concentration was increased when the paleoclimate tended to be arid-hot, thereby promoting dolomite formation and leading to the interbedded deposition of mudstone, dolomitic mudstone and argillaceous dolomite.
(3) Fluctuations in the salinity of water column caused by changes in the sedimentary environment substantially influence the biological composition of endogenous organic matter, and increased water salinity promoted a higher proportion of salt-tolerant algae than to salt-intolerant algae.
(4) The sedimentary period of the P_2p existed in a consistently stable and anoxic environment, which was conducive to the preservation of organic matter. In addition, the increased paleoproductivity resulting from volcanic activities played a pivotal role in promoting organic matter enrichment within the mixed sedimentary rock.

CRediT authorship contribution statement

Wenren Zeng: Investigation, Software, Writing – original draft. **Boran Wang:** Data curation, Writing – original draft, Writing – review & editing. **Xuan Chen:** Data curation, Writing – review & editing. **Guobin Fu:** Writing – review & editing. **Zhihuan Zhang:** Conceptualization, Methodology, Supervision. **Zhilong Huang:** Writing – review & editing.

Declaration of competing interest

The authors hereby affirm that they have no conflicts of interest pertaining to this study. We assert that we possess no business or associated interests that could potentially create a conflict of interest in relation to the submitted work.

Data availability

Data will be made available on request.

Acknowledgements

This study is financially supported by the Ministry of Education Science and Technology Industry-University Cooperation and Education Project (Grant No. KTGSZC2020). The authors sincerely thank the Tuha Oilfield Company of PetroChina Co. Ltd. for providing the cores for this study. Additionally, we express our gratitude to the editors and reviewers for their valuable criticisms, insightful comments and constructive suggestions.

References

Algeo, T.J., Liu, J.S., 2020. A re-assessment of elemental proxies for paleoredox analysis. Chem. Geol. 540, 119549.
Algeo, T.J., Maynard, J.B., 2004. Trace-element behavior and redox facies in core shales of Upper Pennsylvanian Kansas-type cyclothems. Chem. Geol. 206 (3–4), 289–318.

Algeo, T.J., Tribovillard, N., 2009. Environmental analysis of paleoceanographic systems based on molybdenum-uranium covariation. Chem. Geol. 268 (3), 211–225.
Bai, Y.Y., Liu, Z.J., Sun, P.C., Liu, R., Hu, X.F., Zhao, H.Q., Xu, Y.B., 2015. Rare earth and major element geochemistry of Eocene fine-grained sediments in oil shale and coal-bearing layers of the Meihe Basin, Northeast China. J. Asian Earth Sci. 97 (A), 89–101.
Balistrieri, L., Shanks, W., Cuhel, R., Aguilar, C., 2007. The Influence of Sublacustrine Hydrothermal Vent. Fluids on the Geochemistry of Yellowstone Lake: U.S. Geological Survey Professional Paper 1717, 1–30.
Bechtel, A., Jia, J.L., Strobl, S.A.I., Sachsenhofer, R.F., Liu, Z.J., Gratzer, R., Püttmann, W., 2012. Palaeoenvironmental conditions during deposition of the Upper cretaceous oil shale sequences in the Songliao Basin (NE China): Implications from geochemical analysis. Org. Geochem. 46, 76–95.
Bohacs, K.M., Grabowski, G.J., Carroll, A.R., Mankiewicz, P.J., Miskell-Gerhardt, K.J., Schwalbach, J.R., 2005. Production, destruction, and dilution: The many paths to source rock development. In: Harris, N.B. (Ed.), The Deposition of Organic-Carbon-Rich Sediments: Models, Mechanisms, and Consequences, vol. 82. SEPM Spec Publ, pp. 61–101.
Brassell, S.C., Eglinton, G., Maxwell, J.R., Philp, R.P., 1978. Natural background of alkanes in the aquatic environment. Aquatic Pollut. 1978, 69–86.
Calvert, S.E., Pedersen, T.F., 1993. Geochemistry of recent Oxic and Anoxic Marine-Sediments - Implications for the Geological Record. Mar. Geol. 113 (1–2), 67–88.
Chang, X.C., Liu, T.J., Shi, B.B., Zhang, G.L., Yu, H.Z., Chen, G., Zhang, P.F., 2023. The shale oil potential of Permian Lucaogou shales (Southeastern Junggar Basin) evaluated by a new quantitative index based on geochemometric methods. Mar. Pet. Geol. 156, 106434.
Choi, J.H., Hariya, Y., 1992. Geochemistry and depositional environment of Mn oxide deposits in the Tokoro Belt, northeastern Hokkaido, Japan. Econ. Geol. 87, 1265–1274.
Connan, J., Cassou, A.M., 1980. Properties of gases and petroleum liquids derived from terrestrial kerogen at various maturation levels. Geochim. Cosmochim. Acta 44, 1–23.
Cranwell, P., 1977. Organic geochemistry of cam loch (Sutherland) sediments. Chem. Geol. 20, 205–221.
Crerar, D.A., Namson, J., Chyi, M.S., Williams, L., Feigenson, M.D., 1982. Manganiferous cherts of the Franciscan assemblage; I, General geology, ancient and modern analogues, and implications for hydrothermal convection at oceanic spreading centers. Econ. Geol. 77, 519–540.
Cullen, J.T., Field, M.P., Sherrell, R.M., 2001. Determination of trace elements in filtered suspended marine particulate material by sector field HR-ICP-MS. J. Anal. At. Spectrom. 16, 1307–1312.
Davis, R.A., Cuffe, C.K., Kowalski, K.A., Shock, E.J., 2003. Stratigraphic models for microtidal tidal deltas; examples from the Florida Gulf coast. Mar. Geol. 200 (1–4), 49–60.
Demaison, G.T., Moore, G.T., 1980. Anoxic environments and oil source bed genesis. Org. Geochem. 2, 9–31.
Didyk, B.M., Simoneit, B.R.T., Brassell, S.C.T., Eglinton, G., 1978. Organic geochemical indicators of palaeoenvironmental conditions of sedimentation. Nature 272, 216–222.
Ding, W.J., Hou, D.J., Jiang, L., Jiang, Y.H., Wu, P., 2020. High abundance of carotanes in the brackish-saline lacustrine sediments: a possible cyanobacteria source? Int. J. Coal Geol. 219, 103373.
Ding, X.J., Gao, C.H., Zha, M., Chen, H., Su, Y., 2017. Depositional environment and factors controlling β-carotane accumulation: a case study from the Jimsar Sag, Junggar Basin, northwestern China. Palaeogeogr. Palaeoclimatol. Palaeoecol. 485, 833–842.
Ding, X.J., Qu, J.X., Imin, A., Zha, M., Su, Y., Jiang, Z.F., Jiang, H., 2019. Organic matter origin and accumulation in tuffaceous shale of the lower Permian Lucaogou Formation, Jimsar Sag. J. Pet. Sci. Eng. 179, 696–706.
Dorsey, R.J., Kidwell, S.M., 1999. Mixed carbonate-siliciclastic sedimentation on a tectonically active margin, example from the Pliocene of Baja California Sur. Mexico. Geol. 27 (10), 935–938.
Eugster, H.P., Hardie, L.A., 1978. Saline lakes. In: Lerman, A. (Ed.), Lakes: Chemistry, Geology, Physics. Springer, New York, pp. 237–293.
Fagundes, M.B., Falk, R.B., Facchi, M.M.X., Vendruscolo, R.G., Maroneze, M.M., Zepka, L.Q., Jacob-Lope, E., Wagner, R., 2019. Insights in cyanobacteria lipidomics: a sterols characterization from Phormidium autumnale biomass in heterotrophic cultivation. Food Res. Int. 119, 777–784.
Fan, T.T., Liu, Y.Q., Li, H., Che, F.X., Yang, H.K., 2021. Origin and geological significance of analcime-bearing tuffaceous pisolitic limestone: example from Guadalupian Pingdiquan Formation, eastern Junggar Basin. Chin. J. Geol. 56 (4), 1147–1164 (in Chinese with English abstract).
Feng, J.L., Cao, J., Hu, K., Peng, X.Q., Chen, Y., Wang, Y.F., Wang, M., 2013. Dissolution and its impacts on reservoir formation in moderately to deeply buried strata of mixed siliciclastic–carbonate sediments, northwestern Qaidam Basin, Northwest China. Mar. Pet. Geol. 39 (1), 124–137.
Fu, J.M., Sheng, G.Y., Xu, J.Y., Eglinton, G., Gowar, A.P., Jia, R.F., Fan, S.F., Peng, P.A., 1990. Application of biological markers in the assessment of paleoenvironments of Chinese non – marine sediments. Org. Geochem. 16, 769–779.
Grantham, P.J., Wakefield, L.L., 1988. Variations in the sterane carbon number distributions of marine source rock derived crude oils through geological time. Org. Geochem. 12, 61–73.
Hackley, P.C., Fishman, N., Wu, T., Baugher, G., 2016. Organic petrology and geochemistry of mudrocks from the lacustrine Lucaogou Formation, Santanghu Basin, Northwest China: application to lake basin evolution. Int. J. Coal Geol. 168, 20–34.
Hao, F., Zhou, X.H., Zhu, Y.M., Yang, Y.Y., 2011. Lacustrine source rock deposition in response to co–evolution of environments and organisms controlled by tectonic subsidence and climate, Bohai Bay Basin, China. Org. Geochem. 42, 323–339.
Hatch, J.R., Leventhal, J.S., 1992. Relationship between inferred redox potential of the depositional environment and geochemistry of the upper pennsylvanian (Missourian) Stark shale member of the Dennis limestone, Wabaunsee county, Kansas. U.S.A. Chem. Geol. 99, 65–82.
ten Haven, H.L., Leeuw, J.W., Rullkötter, J., Sinninghe Damsté, J.S., 1987. Restricted utility of the pristane/phytane ratio as a palaeoenvironmental indicator. Nature 330, 641–643.
Hedges, J.I., Keil, R.G., 1995. Sedimentary organic matter preservation: an assessment and speculative synthesis. Mar. Chem. 49, 81–115.
Horsfield, B., Curry, D.J., Bohacs, K., Littke, R., Rullkötter, J., Schenk, H.J., Radke, M., Schaefer, R.G., Carroll, A.R., Isaksen, G., Witte, E.G., 1994. Organic geochemistry of freshwater and alkaline lacustrine sediments in the Green River Formation of the Washakie Basin, Wyoming, U.S.A. Organ. Geochem. 1994 22 (3–5), 415–440.
Hou, Y.G., Wang, F.R., He, S., Dong, T., Wu, S.Q., 2017. Properties and shale oil potential of saline lacustrine shales in the Qianjiang Depression, Jianghan Basin, China. Mar. Pet. Geol. 86, 1173–1190.
Hu, T., Pang, X.Q., Jiang, S., Wang, Q.F., Xu, T.W., Lu, K., Huang, C., Chen, Y.Y., Zheng, X.W., 2018a. Impact of paleosalinity, dilution, redox, and paleoproductivity on organic matter enrichment in a saline Lacustrine Rift Basin: a case study of Paleogene organic-rich shale in Dongpu Depression, Bohai Bay Basin, Eastern China. Energy Fuel 32 (4), 5045–5061.
Hu, T., Pang, X.Q., Jiang, S., Wang, Q.F., Zheng, X.W., Ding, X.G., Zhao, Y., Zhu, C.X., Li, H., 2018b. Oil content evaluation of lacustrine organic-rich shale with strong heterogeneity: a case study of the middle Permian Lucaogou formation in Jimusaer sag, Junggar basin, NW China. Fuel 221, 196–205.
Huang, W.Y., Meinschein, W., 1979. Sterols as ecological indicators. Geochem. Cosmochim. Acta 43, 739–745.
ICCP, 1998. The new vitrinite classification (ICCP System 1994). Fuel 77, 349–358.
ICCP, 2001. The new inertinite classification (ICCP System 1994). Fuel 80, 459–471.
Jiang, Y.Q., Liu, Y.Q., Yang, Z., Nan, Y., Wang, R., Zhou, P., Yang, Y.J., Kou, J.Y., Zhou, N.C., 2015. Characteristics and origin of tuff-type tight oil in Jimusaer sag, Junggar Basin, NW China. Pet. Explor. Dev. 42 (6), 810–818.
Jiang, Z.X., Kong, X.X., Yang, Y.P., Zhang, J.G., Zhang, Y.F., Wang, L., Yuan, X.D., 2021. Multi-source genesis of continental carbonate-rich fine-grained sedimentary rocks and hydrocarbon sweet spots. Pet. Explor. Dev. 48 (1), 30–42.
Jin, Z.D., Zhang, E.L., 2002. Paleoclimate implications of Rb/Sr ratios from lake sediments. Sci. Technol. Eng. 2 (3), 20–22 (in Chinese with English abstract).
Jones, B., Manning, D.A.C., 1994. Comparison of geochemical indices used for the interpretation of paleoredox conditions in. Chem. Geol. 111, 111–129.
Katz, B., Lin, F., 2014. Lacustrine basin unconventional resource plays: key differences. Mar. Pet. Geol. 56 (3), 255–265.
Katz, B.J., 2005. Controlling factors on source rock development; a review of productivity, preservation, and sedimentation rate. Soc. Sediment. Geol. 82, 7–16.
Kenward, P.A., Goldstein, R.H., Gonzalez, L.A., Roberts, J.A., 2009. Precipitation of low-temperature dolomite from an anaerobic microbial consortium: the role of methanogenic Archaea. Geobiology 7, 556–565.
Langmann, B., Zakšek, K., Hort, M., Duggen, S., 2010. Volcanic ash as fertiliser for the surface ocean. Atmos. Chem. Phys. 10, 3891–3899.
Lash, G.G., Blood, D.R., 2014. Organic matter accumulation, redox, and diagenetic history of the Marcellus Formation, southwestern Pennsylvania, Appalachian basin. Mar. Pet. Geol. 57, 244–263.
Lerman, A., 1978. Lakes: Chemistry, Geology, Physics. Springer, New York, pp. 237–289.
Lerman, A.D.I., Gat, J. (Eds.), 1989. Physics and Chemistry of Lakes. Springer-Verlag, Berlin.
Li, Q.Q., Xu, S., Hao, F., Shu, Z.G., Chen, F.L., Lu, Y.C., Wu, S.Q., Zhang, L., 2021. Geochemical characteristics and organic matter accumulation of argillaceous dolomite in a saline lacustrine basin: a case study from the paleogene xingouzui formation, Jianghan Basin, China. Mar. Pet. Geol. 128, 105041.
Li, W., Lu, S., Xue, H., Zhang, P., Hu, Y., 2015. Oil content in argillaceous dolomite from the Jianghan Basin, China: application of new grading evaluation criteria to study shale oil potential. Fuel 143, 424–429.
Liu, B., Bechtel, A., Sachsenhofer, R.F., Gross, D., Gratzer, R., Chen, X., 2017. Depositional environment of oil shale within the second member of Permian Lucaogou Formation in the Santanghu Basin, Northwest China. Int. J. Coal Geol. 175, 10–25.
Liu, B., Bechtel, A., Gross, D., Fu, X., Li, X., Sachsenhofer, R.F., 2018. Middle Permian environmental changes and shale oil potential evidenced by high-resolution organic petrology, geochemistry and mineral composition of the sediments in the Santanghu Basin, Northwest China. Int. J. Coal Geol. 185, 119–137.
Liu, G., Zhou, D., 2007. Application of microelements analysis in identifying sedimentary environment-taking Qianjiang Formation in the Jiang Han Basin as an example. Pet. Geol. Exp. 29 (3), 307–311 (in Chinese with English abstract).
Liu, S.J., Gao, G., Jin, J., Gang, W.Z., Xiang, B.L., 2022. Source rock with high abundance of C_{28} regular sterane in typical brackish-saline lacustrine sediments: biogenic source, depositional environment and hydrocarbon generation potential in Junggar Basin, China. J. Pet. Sci. Eng. 208, 109670.
Liu, X.P., Lai, J., Fan, X.C., Shu, H.L., Wang, G.C., Ma, X.Q., Liu, M.C., Guan, M., Luo, Y. F., 2020. Insights in the pore structure, fluid mobility and oiliness in oil shales of Paleogene Funing Formation in Subei Basin, China. Mar. Pet. Geol. 114, 104228.
Luo, X., Wang, Z., Zhang, L., Yang, W., Liu, L., 2007. Overpressure generation and evolution in a compressional tectonic setting, the southern margin of Junggar Basin, northwestern China. AAPG Bull. 91, 1123–1139.

Machel, H.G., 2004. Concepts and models of dolomitization: a critical reappraisal. Geol. Soc. Lond. Spec. Publ. 235, 7–63.
Manche, C.J., Kaczmarek, S.E., 2019. Evaluating reflux dolomitization using a novel high-resolution record of dolomite stoichiometry: a case study from the Creta- ceous of Central Texas, USA. Geology 47 (6), 586–590.
Manche, C.J., Kaczmarek, S.E., 2021. A global study of dolomite stoichiometry and cation ordering through the Phanerozoic. J. Sediment. Res. 91 (5), 520–546.
Marchig, V., Gundlach, H., Möller, P., Schley, F., 1982. Some geochemical indicators for discrimination between diagenetic and hydrothermal metalliferous sediments. Mar. Geol. 50, 241–256.
Martin, J.H., Knauer, G.A., 1973. The elemental composition of plankton. Geochim. Cosmochim. Acta 37, 1639–1653.
Martins, L.L., Schulz, H.M., Severiano Ribeiro, H.J.P., Nascimento, C.A.D., Souza, E.S.D., da Cruz, G.F., 2020. Organic geochemical signals of freshwater dynamics controlling salinity stratification in organic–rich shales in the lower Permian Irati Formation (Paraná Basin, Brazil). Org. Geochem. 140, 103958.
McLennan, S.M., 1989. Rare earth elements in sedimentary rocks: influence of provenance and sedimentary processes. Rev. Mineral. Geochem. 21, 169–200.
Meng, Z.Y., Liu, Y.Q., Jiao, X., Ma, L.T., Zhou, D.W., Li, H., Cao, Q., Zhao, M.R., Yang, Y. Y., 2022. Petrological and organic geochemical characteristics of the Permian Lucaogou Formation in the Jimsar Sag, Junggar Basin, NW China: implications on the relationship between hydrocarbon accumulation and volcanic-hydrothermal activities. J. Pet. Sci. Eng. 210, 110078.
Moldowan, J.M., Seifert, W.K., Gallegos, E.J., 1985. Relationship between petroleum composition and depositional environment of petroleum source rocks. AAPG Bull. 69 (8), 1255–1268.
Moradi, A.V., Sarı, A., Akkaya, P., 2016. Geochemistry of the miocene oil shale (hançili formation) in the Çankırı-Çorum basin, Central Turkey: implications for paleoclimate conditions, source–area weathering, provenance and tectonic setting. Sediment. Geol. 341, 289–303.
Mount, J.F., 1984. Mixing of siliciclastic and carbonate sediments in shallow shelf environments. Geology 12 (7), 432–435.
Murphy, S.M., McCormick, A., Eglinton, G., 1967. Perhydro–beta–Carotene in the Green River Shale. Science (New York, N.Y.) 157, 1040–1042.
Olgun, N., Duggen, S., Andronico, D., Kutterolf, S., Croot, P.L., Giammanco, S., Censi, P., Randazzo, L., 2013. Possible impacts of volcanic ash emissions of Mount Etna on the primary productivity in the oligotrophic Mediterranean Sea: results from nutrient-release experiments in seawater. Mar. Chem. 152, 32–42.
Palermo, D., Aigner, T., Geluk, M., Poeppelreiter, M., Pipping, K., 2008. Reservoir potential of a lacustrine mixed carbonate/siliciclastic gas reservoir: the lower Triassic Rogenstein in the Netherlands. J. Pet. Geol. 31 (1), 61–96.
Pan, Y.S., Huang, Z.L., Li, T.J., Guo, X.B., Xu, X.F., Chen, X., 2020. Environmental response to volcanic activity and its effect on organic matter enrichment in the Permian Lucaogou Formation of the Malang Sag, Santanghu Basin, Northwest China. Palaeogeogr. Palaeoclimatol. Palaeoecol. 560, 110024.
Pan, Y.S., Huang, Z.L., Guo, X.B., Wang, R., Lash, G.G., Fan, T.G., Liu, W.H., 2021. A re-assessment and calibration of redox thresholds in the Permian Lucaogou Formation of Malang Sag, Santanghu Basin, Northwest China. Mar. Pet. Geol. 135, 105406.
Pedersen, T.F., Calvert, S.E., 1990. Anoxia vs. productivity: what controls the formation of organic-carbon-rich sediments and sedimentary rocks? Am. Assoc. Pet. Geol. Bull. 74, 454–466.
Perri, E., Tucker, M.E., Slowakiewicz, M., Whitaker, F., Bowen, L., Perrotta, I.D., 2018. Carbonate and silicate biomineralization in a hypersaline microbial mat (Mesaieed sabkha, Qatar): roles of bacteria, extracellular polymeric substances and viruses. Sedimentology 65 (4), 1213–1245.
Peters, K.E., Cassa, M.R., 1994. Applied source rock geochemistry: Chapter 5: Part II. In: Essential Elements.
Peters, K.E., Walters, C.C., Moldowan, J.M., 2005. The Biomarker Guide. Biomarkers and Isotopes in Petroleum Exploration and Earth History. Cambridge University Press, New York.
Philp, R.P., Gilbert, T.D., 1986. Biomarker distributions in Australian oils predominantly derived from terrigenous source material. Org. Geochem. 10, 73–84.
Pickel, W., Kus, J., Flores, D., Kalaitzidis, S., Christanis, K., Cardott, B.J., Misz-Kennan, M., Rodrigues, S., Hentschel, A., Hamor-vido, M., Crosdale, P., Wagner, N., 2017. Classification of liptinite – ICCP System 1994. Int. J. Coal Geol. 169, 40–61.
Pierret, M.C., Clauer, N., Blanc, G., 2000. Influence hydrothermale dans les sédiments de fosses de la mer rouge par l'étude de quelques éléments traces. Oceanol. Acta 23, 783–792.
Piper, D.Z., Perkins, R.B., 2004. A modern vs. Permian black shale—the hydrography, primary productivity, and water-column chemistry of deposition. Chem. Geol. 206 (3–4), 177–197.
Pisarskii, B.I., Konev, A.A., Levi, K.G., Delvaux, D., 1998. Carbon dioxide-bearing alkaline hydrotherms and strontium-bearing travertines in the songwe river valley (tanzania). Geol. Geofiz. 39 (7), 941–948.
Pujol, F., Berner, Z., Stüben, D., 2006. Palaeoenvironmental changes at the Frasnian/Famennian boundary in key European sections: chemostratigraphic constraints. Palaeogeogr. Palaeoclimatol. Palaeoecol. 240 (1–2), 120–145.
Qian, Q., Gao, J., Klemd, R., He, G., Song, B., Liu, D., Xu, R., 2009. Early Paleozoic tectonic evolution of the Chinese South Tianshan Orogen: constraints from SHRIMP zircon U-Pb geochronology and geochemistry of basaltic and dioritic rocks from Xiate, NW China. Int. J. Earth Sci. 98, 551–569.
Requejo, A.G., Allan, J., Creaney, S., Gray, N.R., Cole, K.S., 1992. Aryl isoprenoids and diaromatic carotenoids in Paleozoic source rocks and oils from the Western Canada and Williston Basins. Org. Geochem. 19, 245–264.
Rodrigues, S., Hernández-Molina, F.J., Larter, R.D., Renesco, M., Hillenbrand, C.-D., Lucchi, G., Rodríguez-Tovar, F.J., 2022. Sedimentary model for mixed depositional systems along the Pacific margin of the Antarctic Peninsula: Decoding the interplay of deep-water processes. Mar. Geol. 445, 106754.
Rohling, E.J., 2000. Paleosalinity: confidence limits and future applications. Mar. Geol. 163, 1–11.
Roser, B.P., Palmer, K., Nathan, S., Cooper, R.A., Tulloch, A.J., 1995. Whole-rock Analyses of Paleozoic Sedimentary Rocks from the Buller and Takaka terranes. Institute of Geological and Nuclear Sciences Report 95/14.
Ryder, R.T., Burruss, R.C., Hatch, J.R., 1998. Black shale source rocks and oil generation in the Cambrian and Ordovician of the central Appalachian Basin, USA. AAPG Bull. 82, 412–441.
Sawyer, E.W., 1986. The influence of source rock type, chemical weathering and sorting on the geochemistry of clastic sediments from the Quetico metasedimentary belt, Superior Province, Canda. Chem. Geol. 55, 77–95.
Scalan, E.S., Smith, J.E., 1970. An improved measure of the odd–even predominance in the normal alkanes of sediment extracts and petroleum. Geochim. Cosmochim. Acta 34, 611–620.
Schoepfer, S.D., Shen, J., Wei, H.Y., Tyson, R.V., Ingall, E., Algeo, T.J., 2015. Total organic carbon, organic phosphorus, and biogenic barium fluxes as proxies for paleo-marine productivity. Earth Sci. Rev. 149, 23–52.
Seifert, W.K., Moldowan, J.M., 1978. Applications of steranes, terpanes and monoaromatics to the maturation, migration and source of crude oils. Geochem. Cosmochim. Acta 42, 77–95.
Shen, J., Schoepfer, S.D., Feng, Q.L., Zhou, L., Yu, J.X., Song, H.Y., Wei, H.Y., Algeo, T.J., 2015. Marine productivity changes during the end-Permian crisis and early Triassic recovery. Earth Sci. Rev. 149, 136–162.
Singh, P., Fillat, M., Kumar, A., 2022. Cyanobacterial Lifestyle and its Applications in Biotechnology. Academic Press.
Sinninghe Damsté, J.S., Kenig, F., Koopmans, M.P., Köster, J., Schouten, S., Hayes, J.M., de Leeuw, J.W., 1995. Evidence for gammacerane as an indicator of water column stratification. Geochim. Cosmochim. Acta 59, 1895–1900.
Slaughter, M., Hill, R.J., 1991. The influence of organic matter in organogenic dolomitization. J. Sediment. Petrol. 61, 296–303.
Song, Y., Li, S., Hu, S., 2019. Warm–humid paleoclimate control of salinized lacustrine organic–rich shale deposition in the Oligocene Hetaoyuan Formation of the Biyang Depression, East China. Int. J. Coal Geol. 202, 69–84.
Song, Y., Cao, Q., Li, S.F., Hu, S.Z., Zhu, K., Ye, X., Wan, L., 2021. Salinized lacustrine organic-rich shale influenced by marine incursions: Algal-microbial community, paleoenvironment and shale oil potential in the Paleogene Biyang Depression, East China. Palaeogeogr. Palaeoclimatol. Palaeoecol. 580, 110621.
Steiner, M., Wallis, E., Erdtmann, B.D., Zhao, Y.L., Yang, R.D., 2001. Submarine –hydrothermal exhalative ore layers in black shales from South China and associated fossils – insights into a lower Cambrian facies and bio-evolution. Palaeogeogr. Palaeoclimatol. Palaeoecol. 169, 165–191.
Sun, F.N., Hu, W.X., Wang, X.L., Cao, J., Fu, B., Wu, H.G., Yang, S.C., 2021. Methanogen microfossils and methanogenesis in Permian lake deposits. Geology 49, 13–18.
Suzuki, N., Ishida, K., Shinomiya, Y., Ishiga, H., 1998. High productivity in the earliest Triassic Ocean: black shales, Southwest Japan. Palaeogeogr. Palaeoclimatol. Palaeoecol. 141, 53–65.
Tang, L., Song, Y., Pang, X.Q., Zhang, Z.X., Guo, Y.C., Zhang, H.A., Pan, Z.H., Jiang, H., 2020. Effects of paleo sedimentary environment in saline lacustrine basin on organic matter accumulation and preservation: a case study from the Dongpu Depression, Bohai Bay Basin, China. J. Pet. Sci. Eng. 185, 106669.
Tao, H.F., Qiu, Z., Qu, Y.Q., Liu, J., Qin, Z., Xie, Z.B., Qiu, J.L., Liu, B., 2022. Geochemistry of Middle Permian lacustrine shales in the Jimusar Sag, Junggar Basin, NW China: Implications for hydrothermal activity and organic matter enrichment. J. Asian Earth Sci. 232, 105267.
Tao, K.Y., Cao, J., Wang, Y.C., Ma, W.Y., Xiang, B.L., Ren, J.L., Zhou, N., 2016. Geochemistry and origin of natural gas in the petroliferous Mahu sag, northwestern Junggar Basin, NW China: carboniferous marine and Permian lacustrine gas systems. Org. Geochem. 100, 62–79.
Tao, S., Xu, Y., Tang, D., Xu, H., Li, S., Chen, S., Liu, W., Cui, Y., Gou, M., 2017. Geochemistry of the Shitoumei oil shale in the Santanghu Basin, Northwest China: implications for paleoclimate conditions, weathering, provenance and tectonic setting. Int. J. Coal Geol. 184, 42–56.
Taylor, S.R., McLennan, S.M., 1985. The Continental Crust: Its Composition and Evolution. Blackwell, Oxford.
Tribovillard, N., Algeo, T.J., Lyons, T., Riboulleau, A., 2006. Trace metals as paleoredox and paleoproductivity proxies: an update. Chem. Geol. 232, 12–32.
Vandeginste, V.R., Reed, S.M.H., Ellam, R.M., Osadetz, K., Roure, F., 2009. Host rock dolomitization and secondary porosity development in the upper Devonian Cairn Formation of the Fairholme carbonate complex (south-West Alberta, Canadian Rockies): Diagenesis and geochemical modelling. Sedimentology 56 (7), 2044–2060.
Volkman, J.K., 1986. A review of sterol markers for marine and terrigenous organic matter. Org. Geochem. 9, 83–99.
Volkman, J.K., Barrett, S.M., Blackburn, S.I., Mansour, M.P., Gelin, F., 1998. Microalgal biomarkers: a review of recent research developments. Org. Geochem. 29, 1163–1179.
Wang, C., Wang, Q.X., Chen, G.J., He, L., Xu, Y., Chen, L.Y., Chen, D.F., 2017. Petrographic and geochemical characteristics of the lacustrine black shales from the Upper Triassic Yanchang Formation of the Ordos Basin, China: implications for the organic matter accumulation. Mar. Pet. Geol. 86, 52–65.
Wang, J.X., Sun, P.C., Liu, Z.J., Li, Y.J., 2021. Characteristics and genesis of lacustrine laminar coal and oil shale: a case study in the Dachanggou Basin, Xinjiang, Northwest China. Mar. Pet. Geol. 126, 104924.
Wang, Y., Xu, S., Hao, F., Lu, Y., Shu, Z., Yan, D., Lu, Y., 2019. Geochemical and petrographic characteristics of Wufeng-Longmaxi shales, Jiaoshiba area, Southwest

China: implications for organic matter differential accumulation. Mar. Pet. Geol. 102, 138–154.
Warren, J.K., 2010. Evaporites through time: Tectonic, climatic and eustatic controls in marine and nonmarine deposits. Earth Sci. Rev. 98, 217–268.
Warren, J.K., 2016. Evaporites. Springer, Berlin.
Wei, W., Algeo, T.J., 2020. Elemental proxies for paleosalinity analysis of ancient shales and mudrocks. Geochim. Cosmochim. Acta 287, 341–366.
Wei, W., Algeo, T.J., Lu, Y., Lu, Y., Liu, H., Zhang, S., Peng, L., Zhang, J., Chen, L., 2018. Identifying marine incursions into the Paleogene Bohai Bay Basin lake system in northeastern China. Int. J. Coal Geol. 200, 1–17.
Wu, F.Y., Yang, Y.H., Mitchell, R.H., Bellatreccia, F., Li, Q.L., Zhao, Z.F., 2010. In situ U–Pb and Nd–Hf–(Sr) isotopic investigations of zirconolite and calzirtite. Chem. Geol. 277, 178–195.
Wu, H.G., Hu, W.X., Cao, J., Wang, X.L., Wang, X.L., Liao, Z.W., 2016. A unique lacustrine mixed dolomitic-clastic sequence for tight oil reservoir within the middle Permian Lucaogou Formation of the Junggar Basin, NW China: Reservoir characteristics and origin. Mar. Pet. Geol. 76, 115–132.
Wu, J., Liang, C., Hu, Z.Q., Yang, R.C., Xie, J., Wang, R.Y., Zhao, J.H., 2019. Sedimentation mechanisms and enrichment of organic matter in the ordovician Wufeng formation- Silurian Longmaxi formation in the Sichuan basin. Mar. Pet. Geol. 101, 556–565.
Xia, L.W., Cao, J., Hu, S.Z., Li, S.F., Shi, C.H., 2019. Organic geochemistry, petrology, and conventional and unconventional hydrocarbon resource potential of Paleogene saline source rocks in eastern China: the Biyang Sag of the Nanxiang Basin. Mar. Pet. Geol. 101, 343–354.
Xia, L.W., Cao, J., Hu, W.X., Zhi, D.M., Tang, Y., Li, E.T., He, W.J., 2021. Coupling of paleoenvironment and biogeochemistry of deep-time alkaline lakes: a lipid biomarker perspective. Earth Sci. Rev. 213, 103499.
Xiang, B.L., Zhou, N., Ma, W.Y., Wu, M., Cao, J., 2015. Multiple-stage migration and accumulation of Permian lacustrine mixed oils in the central Junggar Basin (NW China). Mar. Pet. Geol. 59, 87–201.
Xiao, D., Cao, J., Luo, B., Tan, X.C., Liu, H., Zhang, B.J., Yang, X., Li, Y., 2020. On the dolomite reservoirs formed by dissolution: differential eogenetic vs. hydrothermal in the lower Permian Sichuan Basin, SW China. AAPG Bull. 104 (7), 1405–1438.
Xiao, D., Cao, J., Tan, X.C., Xiong, Y., Zhang, D.F., Dong, G.D., Lu, Z.X., 2021. Marine carbonate reservoirs formed in evaporite sequences in sedimentary basins: a review and new model of epeiric basin-scale moldic reservoirs. Earth Sci. Rev. 223, 103960.
Xiao, W., Han, C., Yuan, C., Sun, M., Lin, S., Chen, H., Li, Z., Li, J., Sun, S., 2008. Middle Cambrian to Permian subduction-related accretionary orogenesis of Northern Xinjiang, NW China: implications for the tectonic evolution of Central Asia. J. Asian Earth Sci. 32, 102–117.
Xie, W.Q., Tan, J.Q., Wang, W.H., Schulz, H.M., Liu, Z.J., Kang, X., Wang, Y., Shahzad, A., Jan, I.U., 2021. Middle Jurassic lacustrine source rocks controlled by an aridification event: a case study in the northern Qaidam Basin (NW China). Int. J. Coal Geol. 242, 103779.
Xie, X.M., Volkman, J.K., Qin, J.Z., Borjigin, T., Bian, L.Z., Zhen, L.J., 2014. Petrology and hydrocarbon potential of microalgal and macroalgal dominated oil shales from the Eocene Huadian Formation, NE China. Int. J. Coal Geol. 124, 36–47.
Yang, S.C., Hu, W.X., Fan, J.X., Deng, Y.Y., 2022. New geochemical identification fingerprints of volcanism during the Ordovician-Silurian transition and its implications for biological and environmental evolution. Earth Sci. Rev. 228, 104016.
Yu, S., Wang, X.L., Xiang, B.L., Ren, J.L., Li, E.T., Wang, J., Huang, P., Wang, G.B., Xu, H., Pan, C.C., 2017. Molecular and carbon isotopic geochemistry of crude oils and extracts from Permian source rocks in the northwestern and central Junggar Basin, China. Org. Geochem. 113, 27–42.
Zeng, W.R., Chen, X., Fu, G.B., Wang, Z.Y., Jin, Y., Chen, X., Wang, B.R., Huang, Z.L., Zhang, Z.H., 2023a. Geochemical characteristics and formation conditions of Permian Pingdiquan formation source rocks in Shishugou Sag, Junggar Basin. J. Northeast Pet. Univ. 47 (2), 70–80 (in Chinese with English abstract).
Zeng, W.R., Zhang, Z.H., Wang, B.R., Chen, X., Zheng, R.H., Fu, G.B., Jin, Y., 2023b. Formation mechanism of organic-rich mixed sedimentary rocks in saline lacustrine basin, Permian Lucaogou Formation, Jimsar Sag, Junggar Basin, Northwest China. Mar. Pet. Geol. 156, 106452.
Zhang, J.Y., Liu, G.D., Cao, Z., Tao, S.Z., Felix, M., Kong, Y.H., Zhang, Y.Y., 2019a. Characteristics and formation mechanism of multi-source mixed sedimentary rocks in a saline lake, a case study of the Permian Lucaogou Formation in the Jimusaer Sag, Northwest China. Mar. Pet. Geol. 102, 704–724.
Zhang, K., Liu, R., Liu, Z.J., Li, B.L., Han, J.B., Zhao, K.A., 2020. Influence of volcanic and hydrothermal activity on organic matter enrichment in the Upper Triassic Yanchang Formation, southern Ordos Basin, Central China. Mar. Pet. Geol. 112, 104059.
Zhang, Q., Yu, Q., Wang, J., Xiao, Y.F., Cheng, J.X., Zhao, A.K., Zhang, B., 2018. Application of ICP-MS to Study the rare Earth Element Characteristics and Sedimentary Environment of Black Shale in the Longmaxi Formation in the Southwestern Sichuan Basin. Rock Mineral Anal. 37, 217–224.
Zhang, S., Wu, T., Zhang, S., Cao, C., Ma, W., Shi, J., Sun, G., 2015. Organofacies and paleoenvironment of lower Carboniferous mudstones (Dishuiquan Formation) in Eastern Junggar, NW China. Int. J. Coal Geol. 150, 7–18.
Zhang, S.M., Cao, Y.C., Liu, K.Y., Jahren, J., Xi, K.L., Zhu, R.K., Yang, T., Cao, X., Wang, W., 2019b. Characterization of lacustrine mixed fine-grained sedimentary rocks using coupled chemostratigraphic-petrographic analysis: a case study from a tight oil reservoir in the Jimusar Sag, Junggar Basin. Mar. Pet. Geol. 99, 453–472.
Zhang, Z.J., Cheng, D.W., Zhou, C.M., Yu, K.H., 2021. Characteristics of fine-grained rocks in the Pingdiquan Formation in well Shishu 1 and their significances for shale oil explorations in northeastern Junggar Basin. Nat. Gas Geosci. 32 (4), 562–576 (in Chinese with English abstract).
Zhao, Z.Y., Zhao, J.H., Wang, H.J., Liao, J.D., Liu, C.M., 2007. Distribution characteristics and applications of trace elements in Junggar basin. Nat. Gas Explorat. Dev. 30, 30–33 (in Chinese with English abstract).
Zhi, D.M., Xiang, B.L., Zhou, N., Li, E.T., Zhang, C.J., Wang, Y.C., Cao, J., 2023. Contrasting shale oil accumulation in the upper and lower sweet spots of the lacustrine Permian Lucaogou Formation, Junggar Basin, China. Mar. Pet. Geol. 150, 106178.
Zou, C.N., Yang, Z., Cui, J.W., Zhu, R.K., Hou, L.H., Tao, S.Z., Yuan, X.J., Wu, S.T., Lin, S. H., Wang, L., Bai, B., Yao, J.L., 2013. Formation mechanism, geological characteristics and development strategy of non-marine shale oil in China. Pet. Explor. Dev. 40 (1), 14–27.